UC-25
LBL-7680

STUDY BY ELASTIC THEORY OF THE CLUSTERING OF SOLUTE ATOMS DURING THE EARLY STAGE OF SOLID SOLUTION DECOMPOSITION

Minghwei Hong
(M. S. thesis)

September 1978

Prepared for the U. S. Department of Energy
under Contract W-7405-ENG-48

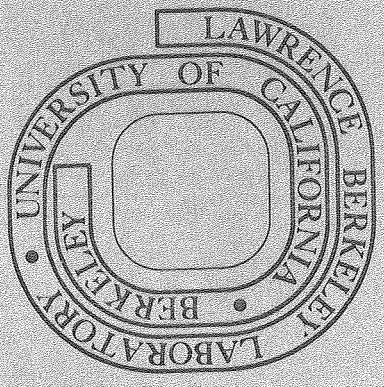

Study by Elastic Theory of the Clustering of Solute Atoms during the Early Stage of Solid Solution Decomposition

Contents

ACKNOWLEDGEMENTS

I would like to thank Professor J. W. Morris, Jr., my benevolent advisor, for his encouragement and support and for his glowing examples of bring forth the scientific truth. His advice, interest and thoughtfulness have been most helpful and are truly appreciated.

I am also grateful to Professor A. G. Khachaturyan for introducing me to the world of elasticity. I would also like to express sincere thanks to Keh-Minn Chang for the discussion and help during the early stages of this work. I am pleased to thank Dr. John L. F. Wang for the discussion of this work from chemistry point of view. I have enjoyed in working with Sheree W. Chen, Kim W. Mahin and Jung-Ihl Kim for interesting discussions.

Most thanks will be given to my close friend Gene Wedge for his collaboration on the case of disk-shaped inclusions with finite thickness and for numerous other fruitful interactions.

Finally, and most importantly, I would like to thank my parents for their encouragement through all these years and Jueinai Kwo, a physicist and my dearest girl friend for her love and very helpful discussion in understanding physics and mathematics.

This work was supported by the Division of Materials Sciences, Office of Basic Energy Sciences, U. S. Department of Energy.

STUDY BY ELASTIC THEORY OF THE CLUSTERING OF SOLUTE ATOMS DURING THE EARLY STAGE OF SOLID SOLUTION DECOMPOSITION

Minghwei Hong

Materials and Molecular Research Division, Lawrence Berkeley Laboratory,
Department of Materials Science and Mineral Engineering
University of California, Berkeley, California 94720

ABSTRACT

Khachaturyan's expression for the elastic strain energy of a coherent inclusion of arbitrary shape in an anisotropic medium is derived from both macroscopic and microscopic theoretical approaches. This expression can be simplified for the case of a very thin disk-shaped inclusion, which enables one to analytically calculate the preferred orientations of Guinier-Preston (G.P.) zones in aluminum-copper alloys and carbide precipitates in iron-carbon martensite. The results are in good agreement with the experimental data. However, this thin plate theory breaks down badly when it is applied to the case of thick plate inclusions, such as the nitride precipitate ($Fe_{16}N_2$) in iron-nitrogen martensite. A method which takes the thickness effects into account has been developed in order to solve this problem. The calculated minimum strain energy orientation of the disk-shaped nitride precipitate in iron-nitrogen martensite, obtained with this method shows excellent agreement with experimental observation.

I. INTRODUCTION

Supersaturated solid solutions usually decompose by a complex precipitation sequence. For example, in aluminum containing a few percent of copper, the generally accepted sequence is:

$$\text{Solid solution} \rightarrow \text{Guinier-Preston (G.P.I) zones} \rightarrow \theta'' \text{ (G.P.II) zones} \rightarrow \theta' \rightarrow \theta\ (CuAl_2) \quad .$$

The term Guinier-Preston (G.P.) zones refers to thin platelets of solute atoms which form during the initial stages of solid solution decomposition in age-hardenable alloys. These solute-rich clusters are usually only several atom layers in thickness and about 20-40Å in diameter. Hence, the initial stages of precipitation are the most difficult to analyze because of the extremely small size of the precipitate particles. The G.P.II zones are only slightly larger than the G.P.I zones and represent a coarsening of the G.P.I zones. These precipitates (G.P.I,II) are coherent with the surrounding matrix, and the strain fields around the precipitates depend on the differences in lattice spacing between the matrix and the precipitate. An additional interphase boundary energy (surface energy) must be associated with these coherent precipitates because of the composition variation across the precipitate-matrix interface. Thus, the orientation and the optimum shape of the precipitate are determined by elastic strain energy and interphase boundary energy. However, in most cases where coherent coupling occurs between the matrix and the precipitate, it is valid to neglect the interphase boundary energy in comparison with that associated with the elastic deformations.

The elastic strain energy of a solid containing precipitates can be divided into two parts: the self energy associated with each precipitate particle, and the interaction energy representing the interaction between the strain fields of neighboring particles. This interaction energy causes the precipitates to lie in periodic arrays, instead of distributing themselves randomly throughout the matrix.[1-9] The self energy of the precipitate depends on the shape, size, orientation of the precipitate, the elastic anisotropy of the system, and the orientational relationship between the lattices of the two phases.

Under the assumption of isotropic elasticity, Eshelby[10-12] was able to calculate the elastic strain energy associated with a coherent ellipsoidal precipitate. In subsequent papers, several authors[13-16] extended Eshelby's work to account for anisotropic media. In 1967, the elastic strain energy of a coherent inclusion with arbitrary shape in an anisotropic medium was solved by Khachaturyan[17] using Fourier Transform techniques under the assumption that the elastic modulus tensors of both the matrix and the precipitate are the same.

For the case of a very thin disk-shaped inclusion, Khachaturyan's formula for the elastic strain energy of an inclusion can be greatly simplified. This simplified form correctly predicts the orientation of thin-plate precipitates in both fcc and bcc lattices, including G.P. zones in aluminum-copper alloys and carbide precipitates which form in iron-carbon martensite during room temperature tempering. There are, however, some cases in which the thin plate theory appears to break down badly. The most important of these, from the engineering point of view, is the case of nitride ($Fe_{16}N_2$) precipitates in

iron-nitrogen martensite. Recent high resolution Transmission Electron Microscopy (TEM) studies reveal one possible source of the discrepancy: the $Fe_{16}N_2$ are observed to form in relatively thick plates. The predictions of the Khachataryan formulation for inclusion of finite thickness have not previously been explored. In the following these equations are shown and compared with experiment[24] for the particular case of $Fe_{16}N_2$ in martensite.

II. THEORETICAL FORMULATION

Khachaturyan's expression for the elastic strain energy can be obtained either from the macroscopic elastic theory (continuous medium)[17] or the continuum limit of the microscopic linear elastic theory for a discrete lattice.[18] The macroscopic theory will be discussed first.

A. Macroscopic Theory

The elastic strain energy per unit volume in a continuous medium can be expressed in the general form

$$f(\underset{\sim}{r}) = f\left(\{\vec{u}(\underset{\sim}{r})\} \quad , \quad \left\{\frac{\partial \vec{u}(\underset{\sim}{r})}{\partial \underset{\sim}{r}}\right\}\right) \tag{2-1}$$

where $\vec{u}(\underset{\sim}{r})$ is the displacement vector, assumed to be a continuous function of $\underset{\sim}{r}$. This form for the free energy is obtained by expanding the vector field $\vec{u}\,(\underset{\sim}{r}')$ about the point $\underset{\sim}{r}$ and neglecting derivatives of second order or higher.

The elastic strain energy f must be invariant under infinitesimal translation, thus

$$f\left(\{\vec{u}(\underset{\sim}{r})\} \quad , \quad \left\{\frac{\vec{u}(\underset{\sim}{r})}{\partial \underset{\sim}{r}}\right\}\right) = f\left(\{\vec{u}(\underset{\sim}{r}) + \vec{a}\} \quad , \quad \left\{\frac{\partial(\vec{u}(\underset{\sim}{r}) + \vec{a})}{\partial \underset{\sim}{r}}\right\}\right) \tag{2-2}$$

where $\vec{a}$ is an arbitrary vector. From this it follows that f is independent of $\vec{u}(\underset{\sim}{r})$. To simplify the notation, define a tensor $u_{ij}(\underset{\sim}{r})$, where

$$u_{ij}(\underset{\sim}{r}) \equiv \frac{\partial u_i(\underset{\sim}{r})}{\partial r_j} \tag{2-3}$$

and a reference state based on the undistorted materials, i.e., f({0}) = 0. Then the total elastic strain energy F can be written

$$F = \int_{\substack{\text{whole}\\ \text{system}}} f(u_{ij}(\underset{\sim}{r}))\, d^3r \quad . \tag{2-4a}$$

Assuming that the function $f(u_{ij}(\underset{\sim}{r}))$ is continuous in u_{ij}, it can be expanded about the reference state $u_{ij} = 0$ to give

$$f(u_{ij}(\underset{\sim}{r})) = \alpha_{ij}u_{ij}(\underset{\sim}{r}) + \frac{1}{2}\lambda_{ij\ell m}u_{ij}(\underset{\sim}{r})\, u_{\ell m}(\underset{\sim}{r}) \tag{2-4b}$$

where α_{ij} and $\lambda_{ij\ell m}$ are material constants and terms of order higher than two have been neglected.

The elementary symmetry properties of α_{ij} and $\lambda_{ij\ell m}$ can be obtained by considering the invariance of f under infinitesimal rotations, i.e.,

$$f(u_{ij}) = f(u_{ij} + \omega_{ij}) \qquad \text{(Appendix 1)} \tag{2-5}$$

where ω_{ij} is an antisymmetric tensor and $(I + \omega_{ij})$ is an infinitesimal rotational operator. Equation (2-5) can be written explicitly as

$$\alpha_{ij}u_{ij} + \frac{1}{2}\lambda_{ij\ell m}\, u_{ij}u_{\ell m} = \alpha_{ij}(u_{ij} + \omega_{ij}) + \frac{1}{2}\lambda_{ij\ell m}(u_{ij}+\omega_{ij})(u_{\ell m}+\omega_{\ell m})$$

Rearranging terms, we get

$$\alpha_{ij}\omega_{ij} + \frac{1}{2}\lambda_{ij\ell m}(u_{ij}\omega_{\ell m} + \omega_{ij}u_{\ell m}) + \frac{1}{2}\lambda_{ij\ell m}\omega_{ij}\omega_{\ell m} = 0 \tag{2-6}$$

Since Eq. (2-6) must be valid for any arbitrary u_{ij} and ω_{ij}, it follows that:

$$\alpha_{ij}\omega_{ij} = 0 \tag{2-7}$$

and

$$\lambda_{ij\ell m}\omega_{ij}\omega_{\ell m} = 0 \ . \tag{2-8}$$

Since ω_{ij} is antisymmetric, from Eq. (2-7), it can be concluded that α_{ij} must be symmetric, i.e.,

$$\alpha_{ij} = \alpha_{ji} \quad . \tag{2-9}$$

By the same argument, it is also clear that

$$\lambda_{ijlm} = \lambda_{jilm} = \lambda_{ijml} = \lambda_{lmij} \quad . \tag{2-10}$$

The tensor u_{ij} may, as is well known, be split into symmetric and antisymmetric tensors:

$$u_{ij} = \varepsilon_{ij} + x_{ij} \quad , \tag{2-11}$$

where $\varepsilon_{ij} = 1/2(u_{ij} + u_{ji})$ is the symmetric tensor and is usually called the strain tensor, and $x_{ij} = 1/2(u_{ij} - u_{ji})$ is the antisymmetric tensor. With the substitution of Eq. (2-11) into Eq. (2-4b), we obtain

$$f(u_{ij}) = \alpha_{ij}(\varepsilon_{ij} + x_{ij}) + \frac{1}{2}\lambda_{ijlm}(\varepsilon_{ij} + x_{ij})(\varepsilon_{lm} + x_{lm}) \quad . \tag{2-12}$$

Using the properties of the symmetric tensor α_{ij}, ε_{ij}, and λ_{ijlm} and the antisymmetric tensor x_{ij}, i.e.,

$$\alpha_{ij}x_{ij} = 0 \quad ,$$

$$\lambda_{ijlm}x_{ij}\varepsilon_{lm} = 0 \quad ,$$

and

$$\lambda_{ijlm}x_{ij}x_{lm} = 0 \quad ,$$

it follows that Eq. (2-12) can be rewritten in the simplified form:

$$f(u_{ij}) = \alpha_{ij}\varepsilon_{ij} + \frac{1}{2}\lambda_{ijlm}\varepsilon_{ij}\varepsilon_{lm} \quad . \tag{2-13}$$

A second order stress tensor can be defined from the above equation;

$$\sigma_{ij} \equiv \frac{\partial f}{\partial \varepsilon_{ij}} = \alpha_{ij} + \lambda_{ijlm}\varepsilon_{lm} \tag{2-14}$$

Now, the elastic strain energy for a coherent inclusion of arbitrary shape in an arbitrary anisotropic medium can be obtained by the method above. For convenience, the diagrams which conceptualize the transformation process are shown in Appendix 2. Following Eshelby,[10] we shall solve this problem with the help of a simple set of imaginary cutting, straining and welding operations. Cut round the region which is to transform and remove it from the matrix (step 1). Allow the unconstrained transformation to take place (step 2). Apply surface tractions chosen so as to restore the region to its original form (step 3). Put the transformed region back in the hole in the matrix (step 4) and let it relax (step 5). From Appendix 2, we see that the total elastic strain energy consists of two terms,

$$F_3 = \frac{1}{2}\lambda_{ijlm}^{(\text{inclusion})}\,\varepsilon_{ij}^{o}\varepsilon_{lm}^{o}\,V \qquad \text{(step 3)}$$

and a relaxation energy term (step 5), where V is the volume of the inclusion. For step 5, we consider the elastic strain energies inside the matrix and the inclusion separately. The elastic strain energy inside the matrix can be expressed as

$$F_5^{(\text{matrix})} = \int_{\text{matrix}} \frac{1}{2}\lambda_{ijlm}^{(\text{matrix})}\,\varepsilon_{ij}(\underset{\sim}{r})\,\varepsilon_{lm}(\underset{\sim}{r})\,d^3r \quad . \tag{2-15}$$

In this case, $\alpha_{ij}^{(\text{matrix})}$ vanishes. Inside the matrix, $\underset{\approx}{\sigma} = 0$ when $\underset{\approx}{\varepsilon} = 0$. Therefore, from Eq. (2-14), it is clear that $\alpha_{ij} = 0$. For the elastic strain energy inside the inclusion, we can write

$$F_5^{(\text{inclusion})} = \int_{\text{inclusion}} \left[\alpha_{ij}\varepsilon_{ij}(\underset{\sim}{r}) + \frac{1}{2}\lambda_{ijlm}^{(\text{inclusion})}\,\varepsilon_{ij}(\underset{\sim}{r})\,\varepsilon_{lm}(\underset{\sim}{r})\right] d^3r \,. \tag{2-16}$$

Inside the inclusion,

$$\sigma_{ij} = -\lambda_{ijlm}^{(\text{inclusion})}\,\varepsilon_{lm}^{o} = -\sigma_{ij}^{o(\text{inclusion})} \quad \text{when} \quad \varepsilon_{ij} = 0 \,.$$

Thus, from Eq. (2-14), it follows that

$$\alpha_{ij} = -\sigma_{ij}^{o(\text{inclusion})} = -\lambda_{ijlm}^{(\text{inclusion})}\,\varepsilon_{lm}^{o} \,. \tag{2-17}$$

Under the assumption that the elastic moduli of both phases are the same, Eqs. (2-15) and (2-16) can be combined into a single equation:

$$\begin{aligned} F_5 &= F_5^{(\text{matrix})} + F_5^{(\text{inclusion})} \\ &= \int \left[-\sigma_{ij}^{o}\theta(\underset{\sim}{r})\,\varepsilon_{ij}(\underset{\sim}{r}) + \frac{1}{2}\lambda_{ijlm}\varepsilon_{ij}(\underset{\sim}{r})\,\varepsilon_{lm}(\underset{\sim}{r})\right] d^3r \end{aligned} \tag{2-18}$$

To obtain Eq. (2-18), Eq. (2-17) was used and a new function called the shape factor $\theta(\underset{\sim}{r})$ was defined such that

$$\theta(\underset{\sim}{r}) = \begin{cases} 1 & \text{inside the inclusion} \\ 0 & \text{otherwise} \end{cases} \tag{2-19}$$

B. Microscopic Theory

Having surveyed the macroscopic theory, it is interesting to study the elastic strain energy from the microscopic (discrete lattice) approach. As argued in Refs. 18-20, the pairwise interaction energies due to elastic deformations can be expressed as

$$\Phi = \Phi_0 + \sum_{\underset{\sim}{R}} \left[\frac{\partial \Phi}{\partial u^i(\underset{\sim}{R})}\right]_{u^i(\underset{\sim}{R})=0} u^i(\underset{\sim}{R}) \qquad (2\text{-}20)$$

$$+ \frac{1}{2} \sum_{\underset{\sim}{R},\underset{\sim}{R}'} \left[\frac{\partial^2 \Phi}{\partial u^i(\underset{\sim}{R})\, \partial u^j(\underset{\sim}{R}')}\right]_{\substack{u^i(\underset{\sim}{R})=0 \\ u^j(\underset{\sim}{R}')=0}} u^i(\underset{\sim}{R})\, u^j(\underset{\sim}{R}')$$

where Φ_0 is the energy of the undeformed solvent lattice containing interstitial atoms. The function $\vec{u}(\underset{\sim}{R})$ is the displacement measured from the position of the lattice site of the pure solvent, and $\underset{\sim}{R}$ determines the position of the primitive cell. Due to the existence of the interstitial atoms, the pure solvent lattice sites will no longer be equilibrium positions. It is assumed that the force at position $\underset{\sim}{R}$ is proportional to the surrounding interstitial atom concentration (an implication of Vegard's Law), i.e.,

$$-\left.\frac{\partial \Phi}{\partial u^i(\underset{\sim}{R})}\right|_{u^i(\underset{\sim}{R})=0} = \sum_{\underset{\sim}{R}',P} F^i_P(\underset{\sim}{R},\underset{\sim}{R}')\, c_p(\underset{\sim}{R}') \qquad (2\text{-}21)$$

where P denotes the interstitial position in one primitive unit cell of the solvent lattice. For convenience, define a tensor $A^{ij}(\underset{\sim}{R},\underset{\sim}{R}')$, such that

$$A^{ij}(\underset{\sim}{R},\underset{\sim}{R}') = \left.\frac{\partial^2 \Phi}{\partial u^i(\underset{\sim}{R})\ \partial u^j(\underset{\sim}{R}')}\right|_{\substack{u^i(\underset{\sim}{R})=0 \\ u^i(\underset{\sim}{R}')=0}} . \tag{2-22}$$

Using Eqs. (2-21) and (2-22), Eq. (2-20) can be rewritten as

$$\Delta\Phi = \Phi - \Phi_0 = -\sum_{p,\underset{\sim}{R},\underset{\sim}{R}'} \left(F_p^i(\underset{\sim}{R},\underset{\sim}{R}')\ u^i(\underset{\sim}{R})\ c_p(\underset{\sim}{R}')\right) + \frac{1}{2}\sum_{\underset{\sim}{R},\underset{\sim}{R}'} A^{ij}(\underset{\sim}{R},\underset{\sim}{R}')\ u^i(\underset{\sim}{R})\ u^j(\underset{\sim}{R}') \quad . \tag{2-23}$$

For crystals having the symmetry property $c_p(\underset{\sim}{R}) = c_p(-\underset{\sim}{R})$, it can be shown (based on work given in Refs. 21 and 22) that

$$\left.\begin{aligned} F_p^i(\underset{\sim}{R},\underset{\sim}{R}') &= F_p^i(\underset{\sim}{R}-\underset{\sim}{R}') \\ A^{ij}(\underset{\sim}{R},\underset{\sim}{R}') &= A^{ij}(\underset{\sim}{R}-\underset{\sim}{R}') \end{aligned}\right\} \tag{2-24}$$

and

$$\left.\begin{aligned} A^{ij}(\underset{\sim}{R}-\underset{\sim}{R}') &= A^{ji}(\underset{\sim}{R}-\underset{\sim}{R}') = A^{ij}(\underset{\sim}{R}'-\underset{\sim}{R}) \\ F_p^i(\underset{\sim}{R}-\underset{\sim}{R}') &= -F_p^i(\underset{\sim}{R}'-\underset{\sim}{R}) \\ \sum_{\underset{\sim}{R}} A^{ij}(\underset{\sim}{R}) &= 0 \quad . \end{aligned}\right\} \tag{2-25}$$

For the continuum approximation, we consider a smooth continuous function $\vec{u}(\underset{\sim}{r})$ which is equal to the discrete function $\vec{u}(\underset{\sim}{R})$ when $\underset{\sim}{r} = \underset{\sim}{R}$. If $\vec{u}(\underset{\sim}{r})$ varies little over the range of $A^{ij}(\underset{\sim}{R}-\underset{\sim}{R}')$, then to an excellent approximation (which becomes exact in the limit of very long-wavelength disturbances) we can make the replacement

$$\vec{u}(\underset{\sim}{R}') = \vec{u}(\underset{\sim}{R}) + [(\underset{\sim}{R}' - \underset{\sim}{R}) \cdot \underset{\sim}{\nabla}]\, \vec{u}(\underset{\sim}{\gamma})\Big|_{\underset{\sim}{\gamma} = \underset{\sim}{R}} . \tag{2-26}$$

Similarly for $Cp(\underset{\sim}{r})$, we have

$$Cp(\underset{\sim}{R}') = Cp(\underset{\sim}{R}) + [(\underset{\sim}{R}' - \underset{\sim}{R}) \cdot \underset{\sim}{\nabla}]\, Cp(\underset{\sim}{\gamma})\Big|_{\underset{\sim}{\gamma} = \underset{\sim}{R}} . \tag{2-27}$$

With the aid of Eq. (2-25), Eq. (2-23) can be rewritten as

$$\begin{aligned}\Delta\Phi = &- \sum_{P,\underset{\sim}{R},\underset{\sim}{R}'} F_p^i(\underset{\sim}{R}-\underset{\sim}{R}')(u^i(\underset{\sim}{R})-u^i(\underset{\sim}{R}'))\, Cp(\underset{\sim}{R}') \\ &- \frac{1}{4}\sum_{\underset{\sim}{R},\underset{\sim}{R}'} (u^i(\underset{\sim}{R}') - u^i(\underset{\sim}{R}))A^{ij}(\underset{\sim}{R}-\underset{\sim}{R}')(u^j(\underset{\sim}{R}') - u^j(\underset{\sim}{R}))\end{aligned} \tag{2-28}$$

Substituting Eqs. (2-26) and (2-27), and again using Eq. (2-25), Eq. (2-28) can be transformed into

$$\begin{aligned}\Delta\Phi = &- \sum_{P,\underset{\sim}{R},\underset{\sim}{R}'} F_p^i(\underset{\sim}{R}')R'^j \frac{\partial}{\partial R^j} u^i(\underset{\sim}{R})\, Cp(\underset{\sim}{R}) \\ &- \frac{1}{4}\sum_{\underset{\sim}{R},\underset{\sim}{R}'} R'^i \frac{\partial}{\partial R^i} u^j(\underset{\sim}{R})\, A^{jm}(\underset{\sim}{R}')\, R'^\ell \frac{\partial}{\partial R^\ell} u^m(\underset{\sim}{R}) \\ = &\sum_{P,\underset{\sim}{R}} \alpha_p^{ij}\, u_{ij}(\underset{\sim}{R})\, Cp(\underset{\sim}{R})\ \ \nu_0 + \frac{1}{2}\sum_{\underset{\sim}{R}} \lambda^{ij\ell m}\, u_{ji}(\underset{\sim}{R})\, u_{m\ell}(\underset{\sim}{R})\, \nu_0\end{aligned} \tag{2-29}$$

where

$$\alpha_p^{ij} = -\frac{1}{\nu_0}\sum_{\underset{\sim}{R}} F_p^i\,(\underset{\sim}{R})\, R^j, \tag{2-30}$$

$$\lambda^{ij\ell m} = -\frac{1}{2}\frac{1}{\nu_0}\sum_{\underset{\sim}{R}} R^i A^{jm}(\underset{\sim}{R})\, R^\ell, \tag{2-31}$$

and ν_0 is the volume of the primitive cell. For the continuum limit, we have

$$\Delta\Phi = \int [\tfrac{1}{2} \lambda^{ij\ell m} u_{ji}(\underset{\sim}{r}) u_{m\ell}(\underset{\sim}{r}) + \sum_p \alpha_p^{ij} u_{ij}(\underset{\sim}{r}) Cp(\underset{\sim}{r})] d^3r \quad (2\text{-}32)$$

For the problem of the inclusion inside the matrix, $Cp(\underset{\sim}{r})$ can be defined in the same manner as the $\theta(\underset{\sim}{r})$ function, i.e.,

$$Cp(\underset{\sim}{r}) = \begin{cases} 1 & \text{inside the inclusion} \\ 0 & \text{otherwise} \end{cases} .$$

Using the same argument as before (from Eq. (2-4a) to Eq. (2-18), the equivalence between Eq. (2-18) and Eq. (2-32) can be established. Demonstrating the equivalence between the microscopic and the macroscopic approaches enables us to better understand the meaning of the assumptions and the extent of the validity of the application.

Taking the sum of the elastic strain energies in steps 3 and 5 (Appendix 2), the total elastic strain energy associated with formation of the elastic inclusion is

$$F = F_0 + \int_{\substack{\text{matrix} + \\ \text{inclusion}}} -\sigma_{ij}^0 \theta(\underset{\sim}{r}) \varepsilon_{ij}(\underset{\sim}{r}) + \tfrac{1}{2} \lambda_{ij\ell m} \varepsilon_{ij}(\underset{\sim}{r}) \varepsilon_{\ell m}(\underset{\sim}{r}) \, d^3r \quad (2\text{-}33)$$

where

$$F_0 \equiv \tfrac{1}{2} \lambda_{ij\ell m} \varepsilon_{ij}^0 \varepsilon_{\ell m}^0 V. \quad (2\text{-}33a)$$

Using the equilibrium condition that the free energy is minimal, hence that $\delta F = 0$ for arbitrary variation of state at constant temperature, we get

$$\delta F = \int [-\sigma_{ij}^0 \theta(\underset{\sim}{r}) \delta(\varepsilon_{ij}(\underset{\sim}{r})) + \tfrac{1}{2} \lambda_{ij\ell m} \delta(\varepsilon_{ij}(\underset{\sim}{r})) \varepsilon_{\ell m}(\underset{\sim}{r}) + \tfrac{1}{2} \lambda_{ij\ell m} \varepsilon_{ij}(\underset{\sim}{r}) \delta(\varepsilon_{\ell m}(\underset{\sim}{r}))] \, d^3r$$

$$= \int [-\sigma^0_{ij}\theta(\underset{\sim}{r}) \frac{\partial}{\partial r_j} (\delta u_i(\underset{\sim}{r})) + \lambda_{ij\ell m} \frac{\partial}{\partial r_j} (\delta u_i(\underset{\sim}{r}))\varepsilon_{\ell m}(\underset{\sim}{r})]d^3r$$

$$= \int \{\sigma^0_{ij}[\frac{\partial}{\partial r_j} \theta(\underset{\sim}{r})]\delta u_i(\underset{\sim}{r}) - \lambda_{ij\ell m} [\frac{\partial}{\partial r_j} \varepsilon_{\ell m}(\underset{\sim}{r})]\delta u_i(\underset{\sim}{r})\}d^3r$$

$$+ \int \{\frac{\partial}{\partial r_j} [-\sigma^0_{ij}\theta(\underset{\sim}{r})\delta u_i(\underset{\sim}{r}) + \lambda_{ij\ell m}\delta u_i(\underset{\sim}{r})\varepsilon_{\ell m}(\underset{\sim}{r})]\}d^3r \ .$$

By Gauss' theorem and by the boundary condition that the displacements on the surface equal zero, the second term can be proved to be zero. This allows us to reduce the above equation to the form

$$\delta F = \int [(\sigma^0_{ij}[\frac{\partial}{\partial r_j} \theta(\underset{\sim}{r})] - \lambda_{ij\ell m}[\frac{\partial}{\partial r_j} \varepsilon_{\ell m}(\underset{\sim}{r})])\delta u_i(\underset{\sim}{r})]d^3r \ .$$

For an arbitrary $\delta u_i(r)$, the validity of $\delta F = 0$ can only hold when

$$\sigma^0_{ij} [\frac{\partial}{\partial r_j} \theta(\underset{\sim}{r})] - \lambda_{ij\ell m} [\frac{\partial}{\partial r_j} \varepsilon_{\ell m}(\underset{\sim}{r})] = 0.$$

The above equation can be rewritten as

$$\lambda_{ij\ell m} (\frac{\partial}{\partial r_j} \frac{\partial}{\partial r_\ell} [u_m(\underset{\sim}{r})]) = \sigma^0_{ij} \frac{\partial}{\partial r_j} \theta(\underset{\sim}{r}) \ . \qquad (2\text{-}34)$$

By utilizing the fourier transformation to κ-space, Eq. (2-34), as shown in Appendix 3, takes the form

$$-(\lambda_{ij\ell m}\kappa_j\kappa_\ell)u_m(\underset{\sim}{\kappa}) = i\sigma^0_{ij}\kappa_j\theta(\underset{\sim}{\kappa}) \ . \qquad (2\text{-}34a)$$

If we denote

$$D_{im} \equiv \lambda_{ij\ell m}\kappa_j\kappa_\ell \ , \qquad (2\text{-}35)$$

Eq. (2-34a) can be rewritten as

$$D_{im}u_m(\underset{\sim}{\kappa}) = -i \sigma^0_{ij}\kappa_j \theta(\underset{\sim}{\kappa}) \qquad (2\text{-}36)$$

or

$$\underset{\approx}{D}|u(\underset{\sim}{\kappa})\rangle = -i\underset{\approx}{\sigma}^0|\kappa\rangle\,\theta(\underset{\sim}{\kappa}) \ . \qquad (2\text{-}36a)$$

From this it follows that the displacement vector in κ-space will be

$$|u(\underset{\sim}{\kappa})\rangle = -i\,\underset{\approx}{D}^{-1}\,\underset{\approx}{\sigma}^0\,|\kappa\rangle\,\theta(\underset{\sim}{\kappa})$$

$$= -i\,\underset{\approx}{G}\,\underset{\approx}{\sigma}^0\,|\kappa\rangle\,\theta(\underset{\sim}{\kappa})$$

where

$$\underset{\approx}{G} \equiv \underset{\approx}{D}^{-1} \text{ is Green's function.} \qquad (2\text{-}37)$$

By the convolution theorem (Appendix 4), Eq. (2-33) can be rewritten as

$$F = F_0 + \int \frac{d^3\kappa}{(2\pi)^3}\left[-\sigma^0_{ij}\,\theta(\underset{\sim}{\kappa})\varepsilon^*_{ij}(\underset{\sim}{\kappa}) + \frac{1}{2}\,\lambda_{ij\ell m}\varepsilon_{ij}(\underset{\sim}{\kappa})\varepsilon^*_{\ell m}(\underset{\sim}{\kappa})\right]$$

$$= F_0 + \int \frac{d^3\kappa}{(2\pi)^3}\left[i\sigma^0_{ij}\theta(\underset{\sim}{\kappa})\,\kappa_i u^*_j(\underset{\sim}{\kappa}) + \frac{1}{2}\,\lambda_{ij\ell m}\kappa_i u_j(\underset{\sim}{\kappa})\kappa_\ell u^*_m(\underset{\sim}{\kappa})\right]$$

(see Appendix 5)

$$= F_0 + \int \frac{d^3\kappa}{(2\pi)^3}\left[i\theta(\underset{\sim}{\kappa})\,\langle\kappa|\underset{\approx}{\sigma}^0|u^*\rangle + \frac{1}{2}\langle u|\,\underset{\approx}{D}\,|u^*\rangle\right]$$

$$= F_0 - \frac{1}{2}\int \frac{d^3\kappa}{(2\pi)^3}\langle\kappa|\underset{\approx}{\sigma}^0\,\underset{\approx}{G}\,\underset{\approx}{\sigma}^0\,|\kappa\rangle\,|\theta(\underset{\sim}{\kappa})|^2 \qquad \text{(see Appendix 6)}$$

$$= \frac{1}{2}\,\lambda_{ij\ell m}\varepsilon^0_{ij}\varepsilon^0_{\ell m}\,V - \frac{1}{2}\int \frac{d^3\kappa}{(2\pi)^3}\langle n|\underset{\approx}{\sigma}^0\,\underset{\approx}{\Omega}\,\underset{\approx}{\sigma}^0|n\rangle\,|\theta(\underset{\sim}{\kappa})|^2 \qquad (2\text{-}38)$$

where

$$\underset{\approx}{\Omega} = |\underset{\sim}{\kappa}|^2\,\underset{\approx}{G}\ , \text{ and } n = \frac{\underset{\sim}{k}}{|\underset{\sim}{k}|}\ .$$

Thus, a very brief and beautiful expression for the elastic strain energy has been obtained which, in κ-space, separates the shape factor

$\theta(\underset{\sim}{\kappa})$, and the function $\langle n|\ \underset{\approx}{\sigma}^0\ \underset{\approx}{\Omega}\ \underset{\approx}{\sigma}^0\ |n\rangle$ which contains the other relevant parameters, such as the stress-free strain ε^0_{ij} and the elastic moduli. Under the assumption that the elastic moduli of both phases are the same, the formula given by Eq. (2-38) can be applied to any system with any structure as a means for calculating the elastic strain energy increase when a coherent inclusion of a new phase possessing arbitrary shape forms in an anisotropic medium.

C. Specific Examples

Now, it is interesting to elucidate some specific applications of this theory.

(I) First, we consider the case in which the matrix has a cubic structure and the stress-free strain tensor is a pure dilation, i.e., $\varepsilon^0_{ij} = \varepsilon^0\delta_{ij}$. For a cubic crystal,[25] the components of the elastic modulus tensor are

$$\left.\begin{aligned} \lambda_{1111} &= \lambda_{2222} = \lambda_{3333} = C11 \\ \lambda_{1122} &= \lambda_{1133} = \lambda_{2233} = C12 \\ \lambda_{1212} &= \lambda_{1313} = \lambda_{2323} = C44 \end{aligned}\right\} \qquad (2\text{-}39)$$

with all other components being equal to zero. From Eq. (2-35), and with the substitution of Eq. (2-39), we get

$$D_{ij}(\underset{\sim}{\kappa}) = \lambda_{i\ell mj}\kappa_\ell\kappa_m = \begin{cases} [n_i^2(C11-C44) + C44]\kappa^2 & \text{when } i = j \\ [n_i n_j(C12+C44)]\kappa^2 & \text{when } i \neq j \end{cases} \qquad (2\text{-}40)$$

It is known that Green's function $\underset{\approx}{G} = \underset{\approx}{D}^{-1}$, and that $\underset{\approx}{\Omega} = |k|^2\ \underset{\approx}{G}$. Therefore, the explicit expression for $\underset{\approx}{\Omega}$ can be obtained by straightforward calculation of $\underset{\approx}{D}^{-1}$.

$$\left.\begin{aligned}\Omega_{11} &= \frac{C11-(C11-C44)n_1^2+\Delta(C11+C12)n_2^2n_3^2}{C44D(\underset{\sim}{n})}\\ \Omega_{12} &= \frac{-(C12+C44)(1+\Delta n_3^2)n_1n_2}{C44D(\underset{\sim}{n})}\end{aligned}\right\} \qquad (2\text{-}41)$$

where

$$D(\underset{\sim}{n}) = C11+\Delta(C11+C12)(n_1^2n_2^2+n_2^2n_3^2+n_3^2n_1^2)+\Delta^2(C11+2C12+C44)n_2^2n_2^2n_3^2 \qquad (2\text{-}41a)$$

and

$$\Delta = \frac{C11-C12-2C44}{C44} \text{ is an anisotropic factor.} \qquad (2\text{-}42)$$

The other components of $\underset{\approx}{\Omega}(\underset{\sim}{n})$ can be obtained from the above equations by cyclic permutation of the cartesian indices.

In this case, $\underset{\approx}{\sigma}^0$ given by Eq. (2-17) can be expressed explicitly as

$$\sigma_{ij}^0 = \lambda_{ij\ell m}\,\varepsilon_{\ell m}^0 = (C11+2C12)\,\varepsilon^0\delta_{ij} \qquad (2\text{-}43)$$

For convenience, we can define $B_1(\underset{\sim}{n}) \equiv \langle n|\underset{\approx}{\sigma}^0\,\underset{\approx}{\Omega}\,\underset{\approx}{\sigma}^0|n\rangle$. Then

$$B_1(\underset{\sim}{n}) = (C11+2C12)^2(\varepsilon^0)^2[\Omega_{11}n_1^2+\Omega_{22}n_2^2+\Omega_{33}n_3^2+2\Omega_{12}n_1n_2+2\Omega_{23}n_2n_3 +2\Omega_{31}n_3n_1] \qquad (2\text{-}44)$$

Substituting Eqs. (2-41) and (2-41a) into Eq. (2-44), $B_I(\underset{\sim}{n})$ becomes

$$B_1(\underset{\sim}{n}) = (C11+2C12)^2(\varepsilon^0)^2 \frac{1+2\Delta(n_1^2n_2^2+n_2^2n_3^2+n_3^2n_1^2)+3\Delta^2n_1^2n_2^2n_3^2}{C11+(C11+C12)\Delta(n_1^2n_2^2+n_2^2n_3^2+n_3^2n_1^2)+(C11+2C12+C44)\Delta^2n_1^2n_2^2n_3^2}\,. \qquad (2\text{-}45)$$

In this case, F_0 given by Eq. (2-33a) can be expressed as

$$F_0^{(I)} = \frac{1}{2}[3(C11+2C12)(\varepsilon^0)^2]\cdot V\,. \qquad (2\text{-}46)$$

Thus, the elastic strain energy of case (I) is now

$$F = F_0^{(I)} - \frac{1}{2}\int \frac{d^3\kappa}{(2\pi)^3} B_1(\underset{\sim}{n})\ |\theta(\underset{\sim}{\kappa})|^2 \tag{2-47}$$

where $F_0^{(I)}$ and $B_1(\underset{\sim}{n})$ are given by Eqs. (2-46) and (2-45) respectively.

(II) As a second example, the matrix is again assumed to have a cubic structure, but the stress-free strain tensor is now assumed to be tetragonal, i.e.

$$\varepsilon_{ij}^0 = \begin{pmatrix} \varepsilon_{11}^0 & 0 & 0 \\ 0 & \varepsilon_{11}^0 & 0 \\ 0 & 0 & \varepsilon_{33}^0 \end{pmatrix} . \tag{2-48}$$

Eqs. (2-39-42) are still applicable in this case, but $\underset{\approx}{\sigma}^0$ has a different form:

$$\sigma_{ij}^0 = \lambda_{ij\ell m}\,\varepsilon_{\ell m}^0 = \begin{pmatrix} (C11+C12)\varepsilon_{11}^0+C12\varepsilon_{33}^0 & 0 & 0 \\ 0 & (C11+C12)\varepsilon_{11}^0+C12\varepsilon_{33}^0 & 0 \\ 0 & 0 & 2C12\varepsilon_{11}^0+C11\varepsilon_{33}^0 \end{pmatrix}. \tag{2-49}$$

Furthermore, σ_{ij}^0 can be divided into two parts: a dilatation part and a deformation part, such that

$$\sigma_{ij}^0 = \sigma^0 \begin{pmatrix} 1 & 0 & 0 \\ 0 & 1 & 0 \\ 0 & 0 & 1 \end{pmatrix} + \tilde{\sigma}^0 \begin{pmatrix} -\frac{1}{2} & 0 & 0 \\ 0 & -\frac{1}{2} & 0 \\ 0 & 0 & 1 \end{pmatrix} \tag{2-50}$$

where

$$\sigma^0 = \frac{C11+2C12}{3}\,(2\varepsilon_{11}^0+\varepsilon_{33}^0) \tag{2-51a}$$

and

$$\tilde{\sigma}^0 = \frac{2(C11-C12)}{3}(-\varepsilon_{11}^0+\varepsilon_{33}^0) \ . \qquad (2\text{-}51b)$$

Using Eqs. (2-41) and (2-49), $B_2(\underset{\sim}{n})$ defined by $\langle n|\underset{\approx}{\sigma}^0 \ \underset{\approx}{\Omega} \ \underset{\approx}{\sigma}^0|n\rangle$ can be expressed as

$$B_2(n) = n_1^2\sigma_{11}^0\Omega_{11}\sigma_{11}^0 + n_2^2\sigma_{22}^0\Omega_{22}\sigma_{22}^0 + n_3^2\sigma_{33}^0\Omega_{33}\sigma_{33}^0 + 2n_1n_2\sigma_{11}^0\Omega_{12}\sigma_{22}^0$$
$$+ 2n_2n_3\sigma_{22}^0\Omega_{23}\sigma_{33}^0 + 2n_3n_1\ \sigma_{33}^0\Omega_{31}\sigma_{11}^0 \ .$$

With the substitution of Eqs. (2-50), (2-51a), (2-51b), (2-41) and (2-41a), $B_2(n)$ becomes

$$B_2(\underset{\sim}{n}) = \frac{(\sigma^0+\tilde{\sigma}^0)^2}{D(\underset{\sim}{n})}[\gamma^2 + An_3^2 - Bn_3^4 + \Delta C n_1^2n_2^2n_3^2 + 2\Delta\gamma^2 n_1^2n_2^2] \qquad (2\text{-}52)$$

where

$$r = \frac{\sigma^0-\frac{1}{2}\tilde{\sigma}^0}{\sigma^0+\tilde{\sigma}^0}$$

$$A = \frac{C11}{C44} + r^2\left(\frac{C11}{C44} - 2\right) - 2r\left(\frac{C12}{C44} + 1\right)$$

$$B = \left(\frac{C11}{C44} - 1\right) + r^2\left(\frac{C11}{C44} - 1\right) - 2r\left(\frac{C12}{C44} + 1\right) \qquad (2\text{-}52a)$$

$$C = \frac{C11+C12}{C44} + 2r^2\left(\frac{C11}{C44} - 1\right) - 4r\left(\frac{C12}{C44} + 1\right) \ .$$

(Note: coefficient C in Reference 17, Eq. 20 was misprinted.)

Similarly,

$$F_0^{(II)} \equiv \frac{1}{2}\lambda_{ij\ell m}\varepsilon_{ij}^0\varepsilon_{\ell m}^0 V$$

$$= \frac{1}{2}[\{2(\varepsilon_{11}^0)^2 + (\varepsilon_{33}^0)^2\}C11 + \{(\varepsilon_{11}^0)^2 + 2\varepsilon_{11}^0\varepsilon_{33}^0\}2C12]V \ . \qquad (2\text{-}53)$$

Therefore, the elastic strain energy of case (II) is

$$F = F_0^{(II)} - \frac{1}{2}\int\frac{d^3\kappa}{(2\pi)^3}B_2(\underset{\sim}{n})|\theta(\underset{\sim}{\kappa})|^2 \qquad (2\text{-}54)$$

where $F_0^{(II)}$ and $B_2(\underset{\sim}{n})$ are given by Eqs. (2-53) and (2-52) respectively.

III. DISK-SHAPED INCLUSIONS

The occurrence of solute atoms clustering during the early stage of solid solution decomposition has been observed in many systems.[9,24,26-33] The shape of the clusters in some systems is spherical, in which case the interphase boundary energy (surface free energy) plays the dominant role. However, the shape of the clusters in some other systems is disk-like, which indicates predominance of the elastic strain energy. The theories discussed in section II can be applied directly to calculate the elastic strain energies and to predict the orientation of these disk-shaped clusters. The displacements around the clusters can also be calculated by using the same theory.

Disk-shaped inclusions with very thin thickness (0-thickness approximation) will be discussed first. The thickness effects will be considered later.

A. 0-Thickness Approximation

If the inclusion is considered to be arbitrarily thin, Eq. (2-38) is found to reduce to a very simple form. For this condition, $\theta(\underset{\sim}{k})$, the Fourier transform of the shape factor $\theta(\underset{\sim}{r})$ becomes a Dirac δ-function i.e., $\theta(k)$ has considerable values only when $\frac{\underset{\sim}{K}}{|\underset{\sim}{K}|} \sim \underset{\sim}{n}$, where $\underset{\sim}{n}$ is the normal to the thin disk-shaped inclusion. Therefore, Eq. (2-38) becomes

$$F = \frac{1}{2}\lambda_{ij\ell m}\varepsilon^0_{ij}\varepsilon^0_{\ell m}V - \frac{1}{2}\langle n|\underset{\approx}{\sigma}^0 \underset{\approx}{\Omega} \underset{\approx}{\sigma}^0|n\rangle \int \frac{d^3k}{(2\pi)^3}\,|\theta(\underset{\sim}{k})|^2$$

$$= \frac{1}{2}\lambda_{ij\ell m}\varepsilon^0_{ij}\varepsilon^0_{\ell m}\,V - \frac{1}{2}\langle n|\underset{\approx}{\sigma}^0 \underset{\approx}{\Omega} \underset{\approx}{\sigma}^0|n\rangle\, V \qquad (3\text{-}1)$$

where

$$\int \frac{d^3k}{(2\pi)^3} |\theta(\underset{\sim}{k})|^2 = \int d^3r[\theta(\underset{\sim}{r})]^2 = \int d^3r\theta(\underset{\sim}{r}) = V. \quad \text{(see Appendix 4)}$$

Following the same argument, the elastic strain energies associated with case I and II in section II (i.e., Eqs. (2-47) and (2-54)) can be simplified respectively to

$$F = F_0^{(I)} - \frac{1}{2} B_1(\underset{\sim}{n})V \tag{3-2}$$

and

$$F = F_0^{(II)} - \frac{1}{2} B_2(\underset{\sim}{n})V \ . \tag{3-3}$$

With the help of Eqs. (3-2) and (3-3), many features of the nucleation of disc-shaped particles can be explained. For a given system, the orientation of the normal of the disk-shaped inclusion is a function of the elastic moduli and the stress-free strains, and the preferred orientation is determined by minimization of the elastic strain energy. The theory can be further used to calculate the displacements around the inclusion, thus providing some comparison with experimental observation.

The thickness effects which influence the preferred orientation and the alignment of the precipitate among the matrix will be discussed below.

B. Finite Thickness Consideration

For the disk-shaped inclusion, $\theta(\underset{\sim}{k})$, the Fourier transform of the shape factor $\theta(\underset{\sim}{r})$, is given as (Appendix 7)

$$\theta(\underset{\sim}{k}) = 2 \cdot V \frac{\sin(|\underset{\sim}{k}| \cdot \cos\alpha \cdot \frac{z_0}{2})}{|\underset{\sim}{k}| \cdot \cos\alpha \cdot \frac{z_0}{2}} \cdot \frac{J_1(|\underset{\sim}{k}| \cdot \sin\alpha \cdot R_0)}{|\underset{\sim}{k}| \cdot \sin\alpha \cdot R_0} \tag{3-4}$$

where V is the volume of the inclusion; J_1 is the Bessel function of the first kind of order 1; R_0 and z_0 are the radius and thickness of the disk-shaped inclusion respectively; and α is the angle between $\underset{\sim}{k}$ and $\underset{\sim}{n}_0$ the normal to the disk. In order to illustrate Eq. (3-4), several plots are shown in Figure 4 giving $\frac{\theta(\underset{\sim}{k})}{V}$ vs. α for various values of $|\underset{\sim}{k}|$, R_0, and z_0.

Since it is impossible to analytically integrate Eqs. (2-47) and (2-54) after inserting Eq. (3-4), the computer has been used to obtain a numerical solution. A survey of the equations of the numerical methods used in the computer calculation is given below.

The general formula by which the elastic strain energy can be obtained has been in Eq. (2-38):

$$F = F_0 - \frac{1}{2}\iiint \langle n|\underset{\approx}{\sigma}^0 \underset{\approx}{\Omega} \underset{\approx}{\sigma}^0|n\rangle \, |\theta(\underset{\sim}{k})|^2 \frac{k^2 dk}{(2\pi)^3} \sin\theta d\theta d\phi. \qquad (3\text{-}5)$$

In this equation, $\langle n|\underset{\approx}{\sigma}^0 \underset{\approx}{\Omega} \underset{\approx}{\sigma}^0|n\rangle$ is a function of θ and ϕ; $|\theta(k)|^2$ is a function of $|\underset{\sim}{k}|$ and α for disk-shaped inclusion; $\cos\alpha = \cos\theta_0\cos\theta + \sin\theta_0 \sin\theta \cos(\phi_0-\phi)$ (Appendix 8); and (θ_0,ϕ_0) determines $\underset{\sim}{n}_0$, the normal to the disk.

The calculation can be simplified by choosing the coordinate (k'_x, k'_y, k'_z) such that $\underset{\sim}{k}'_z \parallel \underset{\sim}{n}_0$. This allows Eq. (3-5) to be rewritten as

$$F = F_0 - \frac{1}{2}\int_0^{\pi}\int_0^{2\pi} \frac{1}{(2\pi)^3} \langle n|\underset{\approx}{\sigma}^0 \underset{\approx}{\Omega} \underset{\approx}{\sigma}^0|n\rangle \sin\alpha d\alpha d\beta \int_0^{\infty} |\theta(\underset{\sim}{k})|^2 k^2 dk \qquad (3\text{-}6)$$

where α and β are the polar angle and the azimuth angle, respectively, in (k'_x, k'_y, k'_z) system.

Denoting

$$f(\alpha) \equiv \int_0^\infty |\theta(\underset{\sim}{k})|^2 k^2 dk \tag{3-7}$$

and

$$B(\alpha,\beta) \equiv \langle n|\underset{\approx}{\sigma}^0 \underset{\approx}{\Omega} \underset{\approx}{\sigma}^0|n\rangle \ , \tag{3-8}$$

Eq. (3-6) becomes

$$F = F_0 - \frac{1}{2} \int_0^\pi \int_0^{2\pi} \frac{1}{(2\pi)^3} B(\alpha,\beta) f(\alpha) \sin\alpha d\alpha d\beta \ . \tag{3-9}$$

The transformation between (k, θ, ϕ) and (k, α, β) can be accomplished by the Euler angles method,[34] i.e.,

$$\underset{\sim}{k}' = \underset{\approx}{R}(\theta_0,\phi_0)\ \underset{\approx}{k} \ , \tag{3-10a}$$

or more explicitly

$$\begin{pmatrix} K_x' \\ K_y' \\ K_z' \end{pmatrix} = \begin{pmatrix} \cos\theta_0\cos\phi_0 & \cos\theta_0\sin\phi_0 & -\sin\theta_0 \\ -\sin\theta_0 & \cos\phi_0 & 0 \\ \sin\theta_0\cos\phi_0 & \sin\theta_0\sin\phi_0 & \cos\theta_0 \end{pmatrix} \begin{pmatrix} K_x \\ K_y \\ K_z \end{pmatrix} \tag{3-10b}$$

Since

$$\underset{\approx}{R}^{-1} = \underset{\approx}{R}^t \ ,$$

$$|\underset{\sim}{K}'|^2 = \underset{\sim}{K}'^t \underset{\sim}{K}' = \underset{\sim}{K}^t\ \underset{\approx}{R}^t\ \underset{\approx}{R}\ \underset{\sim}{K} = \underset{\sim}{K}^t\ \underset{\sim}{K} = |\underset{\sim}{K}|^2$$

i.e., norm of the vector is unchanged during the coordinate transformation. Dividing Eq. (3-10a) by $|\underset{\sim}{K}|$, we get an expression in terms of unit vectors:

$$\underset{\sim}{n}' = \underset{\approx}{R}\ (\theta_0,\phi_0)\ \underset{\sim}{n} \tag{3-11}$$

where $\underset{\sim}{n}' = \frac{\underset{\sim}{k}'}{|\underset{\sim}{k}|}$ and $\underset{\sim}{n} = \frac{\underset{\sim}{k}}{|\underset{\sim}{k}|}$.

The computer calculations used in the following sections are based on the numerical procedures which have been presented above. The elastic strain energy is determined by Eq. (3-9). From the profile of the plot of elastic strain energy vs. orientation, the preferred orientation of a disk-shaped inclusion with considerable thickness can be determined. Specific examples of various precipitates which can be modelled by this approach and comparisons of the model precipitations with experimental data will be discussed in the following two sections.

IV. CUBIC CASE (DISK-SHAPED INCLUSIONS)

In this section, we consider the physical system in which the matrix has a cubic structure and the stress-free strain tensor is a pure dilatation (i.e., $\varepsilon^0_{ij} = \varepsilon^0 \delta_{ij}$). G.P. zones in Al-Cu and Cu-Be alloys are typical examples of thin disk precipitates, which form in a cubic matrix.

It is impossible to measure the stress-free strain ε^0_{ij} of these thin G.P. zones. It is known that the G.P. zones in Al-Cu and Cu-Be alloys are solute-atom-rich regions which are not an equilibrium and ordered phase. Based on these characteristics, it is reasonable to set up the stress-free strain ε^0_{ij} to be cubic rather than tetragonal. The choice of the cubic ε^0_{ij} can be demonstrated to be appropriate by comparing the calculated results such as the strains ε_{ij} and the displacements around these G.P. zones with the experimental observations. One must note the differences between the stress-free strain ε^0_{ij} and the real strains ε_{ij}. ε_{ij} depends on the shape, size and orientation of the inclusion, the function ε^0_{ij} and the elastic moduli while ε^0_{ij} depends only on the differences in lattice spacing between matrix and inclusion. Utilizing the same argument as in Appendix 12 and assuming ε^0_{ij} to be cubic, the strains ε_{ij} inside these thin disk-shaped G.P. zones can be shown to be tetragonal. Consequently, the displacements around these G.P. zones can be obtained and are found to be in good agreement with the experimental data.[28]

By using Eshelby's model and assuming that the platelet of cubic crystal structure and the cubic matrix are infinite in two dimensions and coherently connected, Schwellinger, et al[23] have been able to obtain the preferred orientation of the platelet. By a sequence of plots of

the orientation dependence of the elastic strain energy density, they indicate that plates will lie on the (100) plane when the anisotropic factor Δ given by Eq. (2-42) is less than zero; on the (111) plane when Δ is greater than zero. Using the 0-thickness consideration, Khachaturyan has been able to predict the same results.[5]

A detailed and thorough algebraic calculation based on 0-thickness consideration is given below. From this derivation, it is possible to analytically solve the relationship between the preferred orientation of the thin plate and the anisotropic factor Δ. Furthermore and importantly, this approach can be extended to the case of disk-shaped inclusions with finite thickness. It is found that the results of the 0-thickness consideration are still valid in these more generalized cases. The elastic strain energies and strain fields around the inclusions can also be studied by using the results discussed in Sections II and III.

With the aid of Eqs. (3-2), (2-45) and (2-46), the elastic strain energy in the cubic, 0-thickness case can be computed to be

$$F = \frac{1}{2} V [3(C11+2C12)(\varepsilon^0)^2]$$

$$- \frac{1}{2} V (C11+2C12)^2(\varepsilon^0)^2 \frac{1+2\Delta(n_1^2n_2^2+n_2^2n_3^2+n_3^2n_1^2)+3\Delta^2n_1^2n_2^2n_3^2}{C11+(C11+C12)\Delta(n_1^2n_2^2+n_2^2n_3^2+n_3^2n_1^2)+(C11+2C12+C44)\Delta^2n_1^2n_2^2n_3^2} \quad (4\text{-}1)$$

It can be easily demonstrated that in this case F is a function of the elastic moduli, the volume of the inclusion, the stress-free strain, and the normal $(n_1n_2n_3)$ to the disk-like inclusion. Furthermore, the direction of the normal giving the minimum elastic strain energy depends

only on the elastic moduli. In fact, it can be shown that the determination of the normal depends only on the sign of the anisotropic factor Δ given by Eq. (2-42). The derivation is given in the following algebraic calculations.

To begin with, define a function $A_I(\underset{\sim}{n})$ such that

$$A_I(\underset{\sim}{n}) = \frac{1+2\Delta(n_1^2n_2^2+n_2^2n_3^2+n_3^2n_1^2)+3\Delta^2n_1^2n_2^2n_3^2}{C11+(C11+C12)\Delta(n_1^2n_2^2+n_2^2n_3^2+n_3^2n_1^2)+(C11+2C12+C44)\Delta^2n_1^2n_2^2n_3^2} . \quad (4\text{-}2)$$

Substituting this expression into Eq. (4-1), we get

$$F(\underset{\sim}{n}) = \frac{1}{2} V (C11+2C12)(\varepsilon^0)^2[3-(C11+2C12)A_I(\underset{\sim}{n})] . \quad (4\text{-}3)$$

Since the preferred orientation $\underset{\sim}{n}_0$ will give a minimum value for $F(\underset{\sim}{n}_0)$, it readily follows from Eq. (4-3) that $A_I(\underset{\sim}{n}_0)$ will be a maximum. From the relation

$$n_1^2 + n_2^2 + n_3^2 = 1, \quad (4\text{-}4)$$

it is clear that there are only two independent variables inside $A_I(\underset{\sim}{n})$, i.e., n_1 and n_2. Since $A_I(\underset{\sim}{n})$ is fully symmetric with respect to n_1, n_2 and n_3, any two of them can be chosen as independent variables.

Writing a Taylor expansion for $A_I(n_1,n_2)$ around n_0, $A_I(n_1,n_2)$ can be expressed as

$$A_I(n_1,n_2) = A_I(\underset{\sim}{n}_0) + (n_1-(n_0)_1,\ n_2-(n_0)_2)\begin{pmatrix}\frac{\partial A_I}{\partial n_1}\\ \frac{\partial A_I}{\partial n_2}\end{pmatrix}_{\underset{\sim}{n}=\underset{\sim}{n}_0}$$

$$+\frac{1}{2}(n_1-(n_0)_1,\ n_2-(n_0)_2)\begin{pmatrix}\frac{\partial^2 A_I}{\partial n_1^2} & \frac{\partial^2 A_I}{\partial n_1 \partial n_2}\\ \frac{\partial^2 A_I}{\partial n_1 \partial n_2} & \frac{\partial^2 A_I}{\partial n_2^2}\end{pmatrix}_{\underset{\sim}{n}=\underset{\sim}{n}_0}\begin{pmatrix}n_1-(n_0)_1\\ n_2-(n_0)_2\end{pmatrix}+\cdots \quad (4\text{-}5)$$

The criteria for determining the extrema of $A_I(\underset{\sim}{n})$ are as follows:

$$\text{for } \left(\frac{\partial A_I}{\partial n_1}\right)_{\underset{\sim}{n}=\underset{\sim}{n}_0} = 0,\ \left(\frac{\partial A_I}{\partial n_2}\right)_{\underset{\sim}{n}=\underset{\sim}{n}_0} = 0 \text{ and } \det\begin{pmatrix}\frac{\partial^2 A_I}{\partial n_1^2} & \frac{\partial^2 A_I}{\partial n_1 \partial n_2}\\ \frac{\partial^2 A_I}{\partial n_1 \partial n_2} & \frac{\partial^2 A_I}{\partial n_2^2}\end{pmatrix} > 0 \Bigg\} \quad (4\text{-}6)$$

$$\text{if } \left(\frac{\partial^2 A_I}{\partial n_1^2}\right)_{\underset{\sim}{n}=\underset{\sim}{n}_0} > 0 \Rightarrow A_I(\underset{\sim}{n}_0) \text{ is a local minimum}$$

and

$$\text{if } \left(\frac{\partial^2 A_I}{\partial n_1^2}\right)_{\underset{\sim}{n}=\underset{\sim}{n}_0} < 0 \Rightarrow A_I(\underset{\sim}{n}_0) \text{ is a local maximum.}$$

Taking the partial derivatives of Eq. (4-2) with respect to n_1 and n_2, the following expressions can be obtained

$$\frac{\partial A_I}{\partial n_1} = \frac{2\Delta^4 C44\ n_1(1-2n_1^2-n_2^2)f(n_2)}{[C11+(C11+C12)\Delta(n_1^2n_2^2+n_2^2n_3^2+n_3^2n_1^2)+(C11+2C12+C44)\Delta^2 n_1^2n_2^2n_3^2]^2} \quad (4\text{-}7a)$$

and

$$\frac{\partial A_I}{\partial n_2} = \frac{2\Delta^4 C44\ n_2(1-2n_2^2-n_1^2)f(n_1)}{[C11+(C11+C12)\Delta(n_1^2n_2^2+n_2^2n_3^2+n_3^2n_1^2)+(C11+2C12+C44)\Delta^2 n_1^2n_2^2n_3^2]^2} \quad (4\text{-}7b)$$

where

$$f(n) = -(n^2)^3 + (n^2)^2 + \frac{2C11-2C12-C44}{\Delta^2 C44}(n^2) + \frac{C11-C12}{\Delta^3 C44} . \quad (4\text{-}8)$$

Based on the criteria given by Eq. (4-6), it follows necessarily that

$$n_1(1-2n_1^2-n_2^2)f(n_2) = 0 \quad (4\text{-}9a)$$

and

$$n_2(1-2n_2^2-n_1^2)f(n_1) = 0 . \quad (4\text{-}9b)$$

The possible solutions for the extrema of $A_I(n)$ are

$$\text{(a)} \begin{cases} n_1 = 0 \\ n_2 = 0 \end{cases} \quad \text{i.e., } \underset{\sim}{n}_0 = \{001\}, \quad (4\text{-}10)$$

$$\text{(b)} \begin{cases} n_1 = 0 \\ n_2 = \frac{1}{\sqrt{2}} \end{cases} \quad \text{i.e., } n_0 = \frac{1}{\sqrt{2}}\{011\}, \quad (4\text{-}11)$$

$$\text{(c)} \begin{cases} n_1 = \frac{1}{\sqrt{3}} \\ n_2 = \frac{1}{\sqrt{3}} \end{cases} \quad \text{i.e., } n_0 = \frac{1}{\sqrt{3}}\{111\}, \quad (4\text{-}12)$$

$$(d)\quad \begin{cases} 1 - 2n_1^2 - n_2^2 = 0 \ , \\ f(n_1) = 0 \ . \end{cases} \tag{4-13}$$

and

$$(e)\quad \begin{cases} f(n_1) = 0 \\ f(n_2) = 0 \end{cases} \tag{4-14}$$

The specific cases indicated by Eqs. (4-13) and (4-14) are discussed in Appendix 9. It is shown there that in those specific cases, there are no other possible solutions for the mathematical extrema other than {111}, {001}, and {011}.

The criteria given by (4-6) can be used to explore the maximum and minimum orientations for $F(\underset{\sim}{n})$.

(a) For $\underset{\sim}{n}_0 = \{001\}$

$$\left.\frac{\partial^2 A_I}{\partial n_1^2}\right|_{\underset{\sim}{n}_0 = \{001\}} = 2\Delta \cdot \underbrace{\frac{C11-C12}{(C11)^2}}_{\text{positive number}} \ , \tag{4-15a}$$

$$\left.\frac{\partial^2 A_I}{\partial n_2^2}\right|_{\underset{\sim}{n}_0 = \{001\}} = 2\Delta \cdot \frac{C11-C12}{(C11)^2} \ , \tag{4-15b}$$

and

$$\left.\frac{\partial^2 A_I}{\partial n_1 \partial n_2}\right|_{\underset{\sim}{n}_0 = \{001\}} = 0 \ . \tag{4-15c}$$

Therefore, for $\Delta \neq 0$

$$\det \begin{pmatrix} \frac{\partial^2 A_I}{\partial n_1^2} & \frac{\partial^2 A_I}{\partial n_1 \partial n_2} \\ \frac{\partial^2 A_I}{\partial n_1 \partial n_2} & \frac{\partial^2 A_I}{\partial n_2^2} \end{pmatrix}_{\underset{\sim}{n}_0 = \{001\}} = \left[2\Delta \cdot \frac{C11-C12}{(C11)^2} \right]^2 > 0 . \qquad (4\text{-}16)$$

From this it follows that

$$\text{if } \Delta > 0 \Rightarrow \left. \frac{\partial^2 A_I}{\partial n_1^2} \right|_{\underset{\sim}{n}_0 = \{001\}} > 0 \Rightarrow A_I(\{001\}) \text{ is a local minimum} \qquad (4\text{-}17a)$$

i.e., $F(\{001\})$ is a local maximum,

and

$$\text{if } \Delta < 0 \Rightarrow \left. \frac{\partial^2 A_I}{\partial n_1^2} \right|_{\underset{\sim}{n}_0 = \{001\}} < 0 \Rightarrow A_I(\{001\}) \text{ is a local maximum} \qquad (4\text{-}17b)$$

i.e., $F(\{001\})$ is a local minimum.

(b) For $\underset{\sim}{n}_0 = \frac{1}{\sqrt{2}}\{011\}$

$$\left. \frac{\partial^2 A_I}{\partial n_1^2} \right|_{\underset{\sim}{n}_0 = \frac{1}{\sqrt{2}}\{011\}} = \Delta \underbrace{\left\{ \frac{(C11-C12)^2[(C11-C12)+2C44)}{8(C44)^2[C11+(C11+C12)\frac{\Delta}{4}]^2} \right\}}_{\text{positive number}} \qquad (4\text{-}18a)$$

and

$$\left. \frac{\partial^2 A_I}{\partial n_2^2} \right|_{\underset{\sim}{n}_0 = \frac{1}{\sqrt{2}}\{011\}} = -\Delta \underbrace{\left\{ \frac{4(C11-C12)}{[C11+(C11+C12)\frac{\Delta}{4}]^2} \right\}}_{\text{positive number}} . \qquad (4\text{-}18b)$$

Based on the above results, it directly follows that

$$\det \left(\begin{array}{cc} \dfrac{\partial^2 A_I}{\partial n_1^2} & \dfrac{\partial^2 A_I}{\partial n_1 \partial n_2} \\ \dfrac{\partial^2 A_I}{\partial n_1 \partial n_2} & \dfrac{\partial^2 A_I}{\partial n_2^2} \end{array} \right)_{\underset{\sim}{n}_0 = \frac{1}{\sqrt{2}}\{011\}} < 0 \quad . \tag{4-19}$$

Therefore, for any system, $F(\frac{1}{\sqrt{2}}\{011\})$ is a saddle point of the profile obtained by plotting elastic strain energy vs. orientation.

(c) For $\underset{\sim}{n}_0 = \frac{1}{\sqrt{3}}\{111\}$

$$\left.\frac{\partial^2 A_I}{\partial n_1^2}\right|_{\underset{\sim}{n}_0 = \frac{1}{\sqrt{3}}\{111\}} = \left.\frac{\partial^2 A_I}{\partial n_2^2}\right|_{\underset{\sim}{n}_0 = \frac{1}{\sqrt{3}}\{111\}}$$

$$= - \frac{\frac{8}{3}\Delta^4 \, C44 \, f(\frac{1}{\sqrt{3}})}{\left[C11+(C11+C12)\,\frac{\Delta}{3}+(C11+2C12+C44)\,\frac{\Delta^2}{27}\right]^2}$$

$$= -\Delta \cdot \frac{8}{81\cdot(C44)^2} \cdot$$

$$\underbrace{\left\{ \frac{(C11-C12)\cdot[6(C44)^2+6(C11-C12)C44+2(C11-C12)^2]+2(C44)^3}{[C11+(C11+C12)\cdot\Delta\cdot\frac{1}{3}+(C11+2C12+C44)\cdot\Delta^2\cdot\frac{1}{27}]^2} \right\}}_{\text{positive number}} \tag{4-20}$$

$$\left.\frac{\partial^2 A_I}{\partial n_1 \partial n_2}\right|_{\underset{\sim}{n}_0 = \frac{1}{\sqrt{3}}\{111\}} = \frac{-\frac{4}{3}\Delta^4\, C44\, f(\frac{1}{\sqrt{3}})}{\left[C11+(C11+C12)\,\frac{\Delta}{3}+(C11+2C12+C44)\cdot\frac{\Delta^2}{27}\right]^2} \quad (4\text{-}21)$$

and

$$\det\begin{pmatrix} \frac{\partial^2 A_I}{\partial n_1^2} & \frac{\partial^2 A_I}{\partial n_1 \partial n_2} \\ \frac{\partial^2 A_I}{\partial n_1 \partial n_2} & \frac{\partial^2 A_I}{\partial n_2^2} \end{pmatrix}_{\underset{\sim}{n}_0 = \frac{1}{\sqrt{3}}\{111\}}$$

$$= \left\{ \frac{2\Delta^4\, C44\, f(\frac{1}{\sqrt{3}})}{\left[C11+(C11+C12)\,\frac{\Delta}{3}+(C11+2C12+C44)\,\frac{\Delta^2}{27}\right]^2} \right\}^2 \cdot (\tfrac{16}{9}-\tfrac{4}{9}) > 0 \; . \quad (4\text{-}22)$$

Therefore, we see that

$$\text{if } \Delta > 0 \Rightarrow \left.\frac{\partial^2 A_I}{\partial n_1^2}\right|_{\underset{\sim}{n}_0 = \frac{1}{\sqrt{3}}\{111\}} < 0 \Rightarrow A_I\,(\{111\}) \text{ is a local maximum}$$

i.e., $F(\{111\})$ is a local minimum,

and

$$\text{if } \Delta < 0 \Rightarrow \left.\frac{\partial^2 A_I}{\partial n_1^2}\right|_{\underset{\sim}{n}_0 = \frac{1}{\sqrt{3}}\{111\}} > 0 \Rightarrow A_I\,(\{111\}) \text{ is a local minimum}$$

i.e., $F(\{111\})$ is a local maximum.

As a result of this type of thorough algebraic calculations, it is possible to derive the following results analytically:

(1) for $\Delta > 0$, {111} is the minimum orientation,

(2) for $\Delta < 0$, {001} is the minimum orientation, and

(3) {011} is the saddle point of the elastic strain energy vs. orientation profile in all cases.

These results agree with those of Schwellinger, et al[23] which were obtained diagrammatically using Eshelby's theory.

Now let us look at the more general case of a disk-shaped inclusion of finite thickness. By examining Eqs. (4-1) and (3-4), it is clear that $\langle n|\underset{\approx}{\sigma}^0 \underset{\approx}{\Omega} \underset{\approx}{\sigma}^0|n\rangle$ is fully symmetric with respect to the minimum orientation, i.e., {111} for $\Delta > 0$ and {001} for $\Delta < 0$ as shown in Figure 5 and that $|\theta(k)|^2$ is symmetric with respect to the normal of the disk-shaped inclusion (Figure 4). In view of this symmetry about the minimum energy orientations for the 0-thickness case, there is no reason to expect that the orientation would be different when finite thickness is considered. So the predicted orientation of the disk normal will still be {111} for $\Delta > 0$, or {001} for $\Delta < 0$.

V. TETRAGONAL CASE

The physical system in which the structure of the matrix is cubic and the stress-free strain is tetragonal is studied in this section. An example of such a system is the formation of carbon (or nitrogen) atom clusters in iron-carbon (or iron-nitrogen) martensite during the early stages of precipitation.

It is known that the martensite matrix has a tetragonal structure. During precipitation, segregation of the interstitial atoms occurs. This leads to the formation of regions having a high degree of tetragonality. In other words, the concentration of carbon (or nitrogen) atoms inside the matrix is reduced by precipitation. This reduction in the concentration of carbon (or nitrogen) atoms leads to a reduction in the tetragonality of the matrix. Hence, it is reasonable to assume that the structure of the matrix is now cubic.

Since no experimental data is available for exactly determining the stress-free strain ε^0_{ij} either for the nitride ($Fe_{16}N_2$, Figure 6) in the Fe·N martensite matrix or for the finely dispersed carbide in the Fe·C martensite matrix, the choice of the stress-free strain must be inferred from the results of Bell, Owen[37] and Roberts.[35] To better understand the implications of this choice, a discussion of the derivation is given below.

In Section II Part B--given the microscopic theory approach--we had to assume the validity of Vegard's law in order to derive the continuum limit of the fundamental microscopic theory. Based on this assumption, it is possible to extrapolate the plot of the variation of c and a lattice parameters with changes in carbon (or nitrogen) atom content to include

a broad range of concentrations. It is assumed that this extrapolation is valid in those regions which represent the solute atom concentration inside the precipitate. The appropriateness of this assumption is indicated by the excellent agreement of the normal of the disk-shaped carbide (or nitride) precipitate predicted by this model with that determined by experimental observation. Further confirmation of this assumption can be obtained by comparing the calculated crystal lattice parameters of the ordered ($Fe_{16}N_2$) phase with those based on experimental data (see Appendix 12).

Based on the above discussion and from References 35-39, the following results can be obtained:

For the Fe-C system, the stress-free strain is of the form

$$\varepsilon^0_{ij} = \begin{pmatrix} -0.091 & 0 & 0 \\ 0 & -0.091 & 0 \\ 0 & 0 & 0.858 \end{pmatrix} X_c \quad . \tag{5-1}$$

The observations and characteristics of these carbon atom clusters are discussed in more detail in References 9, 36, 44-47. For the Fe-N system, the stress-free strain is given as

$$\varepsilon^0_{ij} = \begin{pmatrix} -0.095 & 0 & 0 \\ 0 & -0.095 & 0 \\ 0 & 0 & 0.855 \end{pmatrix} X_N \quad . \tag{5-2}$$

In this system, the nitrogen atom cluster inside the Fe-N martensite matrix is found to be an ordered phase ($Fe_{16}N_2$, Figure 6) with the tetragonality along the c-axis.[39] Here, X_c and X_N correspond respectively to the atom fraction of carbon and nitrogen atoms.

As discussed above, the martensite matrix is assumed to have an approximately cubic structure. With this cubic matrix and the stress-free strains given by Eqs. (5-1) and (5-2), we are able to use the results in Section II Part C Case (II) to explore the features of the early stage precipitation in Fe-C (or Fe-N) martensite.

For the Fe-C system, a simplified form of Khachaturyan's solution for the elastic strain energy of a thin plate based on 0-thickness considerations can be applied to analytically calculate the preferred orientation of the carbide precipitates in this martensite matrix. The results are in good agreement with the experimental data. However this thin plate theory breaks down badly when it is applied to the Fe-N system. The nitride ($Fe_{16}N_2$) precipitates have been observed experimentally in recent high resolution Transmission Electron Miscoscopy studies to form in relatively thick plates.[24] Therefore, in order to compute the preferred orientation of a thick Fe-N plate, it is necessary to solve the anisotropic elastic model for the case of a plate of finite thickness. The formulations and the computation procedures used to carry out the required numerical integrations are described in Section III. Based on the calculated results, the preferred orientation is found to be a function of the aspect ratio ($Z_0/2R_0$), where Z_0 and R_0 are the thickness and radius of the disk-shaped inclusion respectively. The results of the thicker plate calculation are in agreement with experimental observation.[24]

Now, let us study the precipitation in the Fe-C system by using 0-thickness approximation and that in the Fe-N system by considering finite thickness effects:

(1) Fe-C system

In the Fe-C system, the elastic strain energy given by Eqs. (3-3), (2-52), (2-52a) and (2-53) under 0-thickness consideration has the form

$$F = \frac{1}{2}\left[(2(\varepsilon_{11}^0)^2+(\varepsilon_{33}^0)^2)\cdot C11+2\cdot((\varepsilon_{11}^0)^2+2\varepsilon_{11}^0\cdot\varepsilon_{33}^0)\cdot C12\right]\cdot V$$

$$- \frac{1}{2}(\sigma_0 + \tilde{\sigma}_0)^2 A_{II}(\underset{\sim}{n})V \qquad (5\text{-}3)$$

where

$$A_{II}(\underset{\sim}{n}) = \frac{r^2+ An_3^2-Bn_3^4+\Delta Cn_1^2n_2^2n_3^2+2\Delta r^2n_1^2n_2^2}{C11+(C11+C12)\Delta(n_1^2n_2^2+n_2^2n_3^2+n_3^2n_1^2)+(C11+2C12+C44)\Delta^2n_1^2n_2^2n_3^2} \qquad (5\text{-}3a)$$

From Eqs. (5-3) and (5-3a), it readily follows that the preferred orientation $\underset{\sim}{n}_0$ will minimize $F(\underset{\sim}{n})$, when $\underset{\sim}{n} = \underset{\sim}{n}_0$ and will maximize $A_{II}(\underset{\sim}{n})$, when $\underset{\sim}{n} = \underset{\sim}{n}_0$.

The problem of maximization of $A_{II}(\underset{\sim}{n})$ is more complicated than the maximization of $A_I(\underset{\sim}{n})$. Therefore, a special technique must be used to deal with this problem. For a fixed value of n_3, $A_{II}(\underset{\sim}{n})$ is the function of n_1 and n_2. Using the relation $n_1^2+n_2^2+n_3^2 = 1$, we can reduce the number independent variables in $A_{II}(\underset{\sim}{n})$ to one. By defining

$$H(n_3) \equiv 1-n_3^2 = n_1^2+n_2^2 \qquad (5\text{-}4)$$

and by setting

$$\left.\begin{aligned} a(n_3) &= C11 + \Delta(C11+C12)\, n_3^2\,(1-n_3^2) \\ b(n_3) &= \Delta(C11+C12) + \Delta^2\,(C11+2C12+C44)n_3^2 \\ e(n_3) &= r^2 + An_3^2 - Bn_3^4 \\ f(n_3) &= \Delta\cdot C\cdot n_3^2 + 2\Delta\cdot r^2 \end{aligned}\right\} \qquad (5\text{-}5)$$

the expression for $A_{II}(n)$ can be rewritten as

$$A_{II}(n) = \frac{e + f\,H\,n_1^2 - f\,n_1^4}{a + b\,H\,n_1^2 - b\,n_1^4} \quad . \tag{5-6}$$

The first derivative of $A_{II}\ (n_1;n_3)$ with respect to n_1 is

$$\frac{dA_{II}(n_1;n_3)}{dn_1} = \frac{2n_1(H-2n_1^2)(af-eb)}{[a+bHn_1^2-bn_1^4]^2} \quad . \tag{5-7}$$

The condition for determining the extrema is

$$\frac{dA_{II}}{dn_1} = 0 \ . \tag{5-8}$$

Evaluating Eq. (5-8), it follows that two solutions exist, either $n_1 = 0$ or $n_1^2 = \frac{H}{2}$. Of course, this is based on the condition that $af-eb \neq 0$. Here, it should be noted that either (ohl) or (hol) corresponds to the $n_1 = 0$ case and that (hhl) corresponds to the $n_1^2 = \frac{H}{2}$ case. From Eq. (5-3a), it readily follows that $A_{II}(\underset{\sim}{n})$ is symmetric with respect to n_1 and n_2. The minimum or maximum conditions can be determined only after the second derivative is examined. The second derivatives of $A_{II}(n_1)$ for $n_1 = 0$ and $n_1^2 = \frac{H}{2}$ are respectively,

$$\left.\frac{d^2A_{II}(n_1;n_3)}{dn_1^2}\right|_{n_1 = 0} = \left(\frac{2H}{a^2}\right)(af-eb) \tag{5-9}$$

and

$$\left.\frac{d^2A_{II}(n_1;n_3)}{dn_1^2}\right|_{n_1^2=\frac{H}{2}} = \frac{2H}{(a+\frac{b}{4}H^2)^2}[-(af-eb)] \ . \qquad (5\text{-}10)$$

From Eqs. (5-9) and (5-10), it follows that

(I) if (af-eb) > 0, then (hhl) maximizes $A_{II}(\underset{\sim}{n})$ and as a consequence minimizes F(n); (5-11)

(II) by the same argument, if (af-eb) < 0, then either (ohl) or (hol) will minimize $F(\underset{\sim}{n})$. (5-12)

From the above discussions, it is agreed that it is extremely important to examine the properties of (af-eb). For this purpose, define a function $W(n_3) \equiv$ af-eb. Substituting Eq. (5-5) for (af-eb), we have

$$\begin{aligned} W(n_3) = {} & [\Delta r^2(C11-C12)]+[\Delta^2 r^2(C11-C44)+\Delta(C\cdot C11-A(C11+C12))]n_3^2 \\ & + \Delta^2[(C11+C12)\cdot(C-2r^2+\tfrac{B}{\Delta})-A\,(C11+2C12+C44)]n_3^4 \\ & + \Delta^2[B(C11+2C12+C44)-C(C11+C12)]n_3^6 \ . \end{aligned} \qquad (5\text{-}13)$$

With the aid of Eqs. (5-1) and (2-52a) as well as Appendix 10 and by setting y equal to n_3^2, Eq. (5-13) can be rewritten numerically for the Fe-C system, where

$$W(n_3) = W(y) = -0.254 + 1.461\ y - 0.691\ y^2 - 4.593\ y^3 \qquad (5\text{-}14)$$

and

$$0 \leqslant y \leqslant 1 \ .$$

From Figure 7, we see that $W(y) \leqslant 0$ in the range $0 \leqslant y \leqslant 1$. The plot as shown in Figure 7 is accurate to within a factor of 10^{-3}. Therefore, from (5-12) and (5-14) it clearly follows that either (hol) or (ohl) is

the minimum orientation. Furthermore, the numerical values of h and l can be obtained by considering the case in which

$$A_{II}(hol) = A_{II}(n_1 0 n_3) = \frac{r^2 + A\, n_3^3 - B n_3^4}{C11 + (C11+C12)\Delta(1-n_3^2)n_3^2} \quad . \tag{5-15}$$

Here, the relation $n_1^2 + n_3^2 = 1$ is used. To determine the extrema of $A_{II}(\underset{\sim}{n})$, set $\frac{dA_{II}}{dn_3} = 0$. Solving for this case, we find that either

$$n_3 = 0 \tag{5-16a}$$

or

$$[C11 \cdot A - \Delta \cdot (C11+C12) \cdot r^2] + 2[\Delta(C11+C12)r^2 - B \cdot C11]n_3^2$$

$$+ [\Delta(C11+C12)(A-B)]n_3^4 = 0 \tag{5-16b}$$

Examining the second derivative of $A_{II}(n_1 0 n_3)$ when $n_3 = 0$, we obtain for the Fe-C system:

$$\left(\frac{d^2 A_{II}}{dn_3^2}\right)_{n_3 = 0} = \frac{C11 \cdot A - \Delta \cdot r^2 \cdot (C11+C12)}{(C11)^2} > 0 \quad . \tag{5-17}$$

Therefore, $A_{II}(n_3 = 0)$ is a minimum and consequently $F(n_3 = 0)$ is a maximum. Thus, the solution obtained in Eq. (5-16b) will minimize $F(\underset{\sim}{n})$ and for the Fe-C system, Eq. (5-16b) can be rewritten in numerical form as

$$-3.356\, n_3^4 + 1.953\, n_3^2 + 0.84 = 0 \quad . \tag{5-18}$$

By solving this equation, we find that $n_3^2 = 0.87$ (i.e., $n_3 = 0.933$)

and that $n_1^2 = 0.13$ (i.e., $n_1 = 0.361$).

Using the 0-thickness approximation, the theoretical prediction for the normal of the clusters in the Fe-C system is $n_0 = (0.361, 0, 0.933)$. Within experimental error, the result is in good agreement with the experimental data.[9] Furthermore, the elastic strain energy and fields associated with the carbon atom clusters inside the Fe-C martensite can be easily calculated by the 0-thickness consideration.

(2) Fe-N system

In comparison, based on experimental evidence, it is not appropriate to apply 0-thickness approximation to the Fe-N system. The thickness effect must be taken into account. For disk-shaped inclusions, the problem can be solved numerically with the aid of a computer. The calculation procedure has been described in section III, Part B. The results are presented in Table I. It is found that the aspect ratio $Z_0/2R_0$, plays an important role in determining the preferred orientation of the disk normal. The normal itself is found by minimizing the elastic strain energy function $F(\underset{\sim}{n})$. When $Z_0/2R_0 \geq 1/11.34$ the disk normal is the [001] direction. However, when $Z_0/2R_0 < 1/11.34$, this orientation changes.

In the Fe-N system, the normal obtained using the 0-thickness approximation is found to be (0.382, 0, 0.924) [Appendix 11]. However, the observed normal is (001). This normal can be obtained by including the finite thickness consideration ($Z_0/2R_0 \geqslant 1/11.34$). This claim can be readily demonstrated by examining Figures 4 and 8 and Eq. (3-5). Figure 8 is a plot of $B(\theta,\phi) \equiv \langle n|\underset{\approx}{\sigma}^0 \underset{\approx}{\Omega} \underset{\approx}{\sigma}^0|n\rangle$ vs. θ for the Fe-N system. $|\theta(k)|^2$ is symmetric with respect to the normal of the disk and the

width of the curve becomes increasingly broader as the disk thickens. $B(\theta,\phi)$ is asymmetric with respect to the minimum point (0.382, 0, 0.924), and smaller values of the function occur near (001). Therefore, for the very thin disk with the δ-function $|\theta(\underset{\sim}{k})|^2$ the orientation for the minimum energy lies near (0.382, 0, 0.924), while for the thicker disk with the broader width of the function $|\theta(\underset{\sim}{k})|^2$, the orientation for the minimum energy will be shifted to (001). This normal (001) is in complete agreement with the experimental observation.[24]

VI. DISCUSSION

Comparing with the other theories of elastic strain energy, Khachaturyan's approach provides a brief and simple method with very clear physical concepts. In the k-space calculations, the formula separates the shape factor $\theta(\underset{\sim}{k})$ from the other relevant parameters, such as the elastic constants, the stress-free strain, etc. The formula is also very powerful. It can be applied to any shape of inclusion inside any arbitrary anisotropic medium. For most of the complicated systems, the analytical solutions are almost impossible. However, the results can be obtained numerically via computer calculation. Khachaturyan's formula also makes it possible to study the interaction between the strain fields of neighboring inclusions. The applicability of this approach is limited, however, by the assumption that the elastic moduli of both phases are the same. Therefore, the extending of Khachaturyan's theory to remove this assumption is an important task.

In Reference 18, Khachaturyan already mentioned briefly the result of the continuum limit of the microscopic linear elastic theory. In Section II Part B, we give a detailed and thorough derivation of the continuum limit from the fundamental elastic energy expression given by Eq. (2-20). From this derivation, we have the better understanding on the assumptions made in Khachaturyan's approach.

Based on elastic strain energy expression given by Eq. (2-38), we are able to derive analytically the preferred orientations of very thin disk-shaped inclusions in the cubic case (Section IV) or the tetragonal case (section V). These results can be obtained by the other theories, but not analytically. Furthermore, we are able to calculate the

preferred orientations and the elastic strain energies of the thick disk-shaped precipitates: For the cubic case, the preferred orientations of these thicker plates can be predicted by symmetry argument on Eq. (3-5). For the tetragonal case such as nitride precipitates in the Fe-N martensite, the preferred orientation is found to be a function of the aspect ratio ($Z_0/2R_0$) and the normal (001) can be obtained when the aspect ratio is larger than some critical value. The features of thick disk-shaped precipitates obtained in this work have not been done before.

From the discussions in Section V, an interesting and significant experiment can be proposed. By controlling the aging temperature and the aging time, a series of different thickness of disk-shaped nitride precipitates can be produced. The orientations and thicknesses of those precipitates may be revealed by high resolution transmission Electron Microscopy studies. If results can be obtained in this manner, not only can the phenomena associated with the early stage of nitride precpiptation in a martensite matrix be more fully understood, but also these results will provide a further prolative test for the anisotropic elastic model (Khachaturyan's approach) as a theoretical tool for predicting and understanding precipitation processes in solids.

Further refinements of the theory should include 1) incorporation of variations in elastic moduli, 2) some accounting for the interactions between the strain fields of neighboring inclusions, and 3) application of the microscopic theory (especially where the precipitates are so small as to approach inter-atomic dimensions). It is anticipated that improvements both in the theory and in experimental observation will lead to even stronger agreement than is demonstrated here.

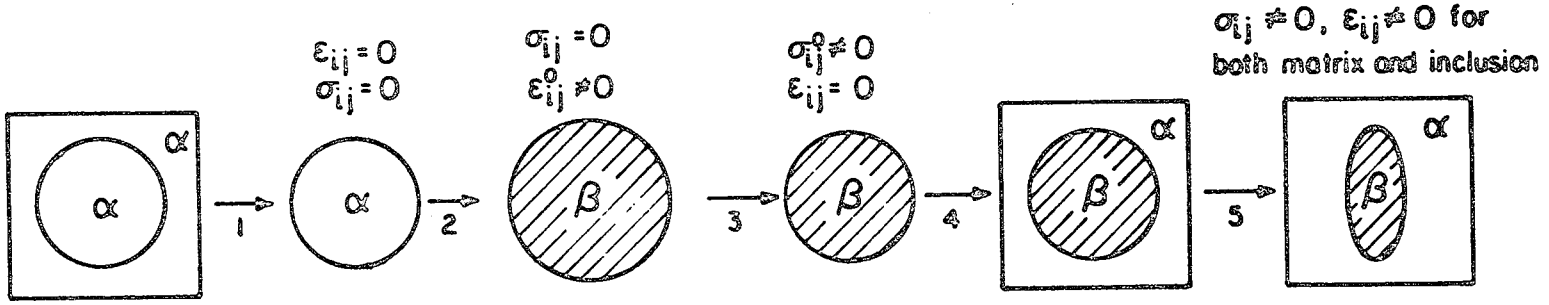
α
α
1
$\varepsilon_{ij} = 0$
$\sigma_{ij} = 0$
α
2
$\sigma_{ij} = 0$
$\varepsilon^0_{ij} \neq 0$
β
3
$\sigma^0_{ij} \neq 0$
$\varepsilon_{ij} = 0$
β
4
α
β
5
$\sigma_{ij} \neq 0$, $\varepsilon_{ij} \neq 0$ for
both matrix and inclusion
α
β

XBL 785-5008

4. Convolution Theorem

$$\int f(\underset{\sim}{r})g(\underset{\sim}{r})d^3\gamma = \int d^3\gamma\left[\frac{d^3k}{(2\pi)^3}\tilde{f}(\underset{\sim}{k})\, e^{i\underset{\sim}{k}\cdot\underset{\sim}{\gamma}}\right]\left[\int\frac{d^3k'}{(2\pi)^3}\tilde{g}(\underset{\sim}{k}')\, e^{i\underset{\sim}{k}'\cdot\underset{\sim}{\gamma}}\right]$$

$$= \iint\frac{d^3k\, d^3k'}{(2\pi)^6}\tilde{f}(\underset{\sim}{k})\,\tilde{g}(\underset{\sim}{k}')\underbrace{\int e^{i(\underset{\sim}{k}+\underset{\sim}{k}')\cdot\underset{\sim}{\gamma}}\, d^3\gamma}_{(2\pi)^3\,\delta(\underset{\sim}{k}+\underset{\sim}{k}')}$$

$$= \int\frac{d^3k}{(2\pi)^3}\tilde{f}(\underset{\sim}{k})\,\tilde{g}(-\underset{\sim}{k})$$

$$= \int\frac{d^3k}{(2\pi)^3}\tilde{f}(\underset{\sim}{k})\,\tilde{g}^*(\underset{\sim}{k})$$

5. $\varepsilon_{ij} = \frac{1}{2}(u_{ij} + u_{ji})$

In k-space, the above equation becomes

$$\varepsilon_{ij}(\underset{\sim}{k}) = \frac{i}{2}(k_i u_j(\underset{\sim}{k}) + k_j u_i(\underset{\sim}{k}))$$

The complex conjugate of $\varepsilon_{ij}(\underset{\sim}{k})$ is

$$\varepsilon^*_{ij}(\underset{\sim}{k}) = -\frac{i}{2}(k_i u^*_j(\underset{\sim}{k}) + k_j u^*_i(\underset{\sim}{k}))$$

$$\sigma^0_{ij}\varepsilon^*_{ij}(k) = -i\sigma^0_{ij}k_i u^*_j(\underset{\sim}{k})$$

$$\lambda_{ij\ell m}\,\varepsilon_{ij}(\underset{\sim}{k})\,\varepsilon^*_{\ell m}(\underset{\sim}{k}) = \lambda_{ij\ell m}\,k_i u_j(\underset{\sim}{k})k_\ell u^*_m(\underset{\sim}{k})$$

6. $|u\rangle = -i \underset{\approx}{G} \underset{\approx}{\sigma}^0 |k\rangle \theta(\underset{\sim}{k})$

$|u^*\rangle = i \underset{\approx}{G} \underset{\approx}{\sigma}^0 |k\rangle \theta^*(\underset{\sim}{k})$

$$i\theta(\underset{\sim}{k}) \langle k|\underset{\approx}{\sigma}^0|u^*\rangle = i\theta(\underset{\sim}{k}) \langle k|\underset{\approx}{\sigma}^0 \underset{\approx}{G} \underset{\approx}{\sigma}^0|k\rangle \theta^*(\underset{\sim}{k})$$

$$= -\langle k|\underset{\approx}{\sigma}^0 \underset{\approx}{G} \underset{\approx}{\sigma}^0|k\rangle |\theta(\underset{\sim}{k})|^2$$

$$\frac{1}{2}\langle u|\underset{\approx}{D}|u^*\rangle = \frac{1}{2}\langle k|(-i)\underset{\approx}{\sigma}^0 \underset{\approx}{G}^0 \theta(\underset{\sim}{k}) \underset{\approx}{D} (i) \underset{\approx}{G} \underset{\approx}{\sigma}^0 \theta^*(\underset{\sim}{k})|k\rangle$$

$$= \frac{1}{2}\langle k|\underset{\approx}{\sigma}^0 \underset{\approx}{G}^0 \underset{\approx}{\sigma}^0|k\rangle |\theta(k)|^2$$

7. The expression for $\theta(\underset{\sim}{k})$, the Fourier transform of shape factor $\theta(\underset{\sim}{r})$, for the disk-shaped inclusion with radius R_0 and thickness Z_0 (Figure 1) will be derived here.

For primed system (x', y', z') (Figure 2),

$$\theta(\underset{\sim}{k}) = \int e^{i\underset{\sim}{k}\cdot\underset{\sim}{\gamma}'} \theta(\gamma') \, d^3\gamma'$$

where

$$\theta(\gamma') = \begin{cases} 1 & \text{inside the inclusion} \\ 0 & \text{otherwise} \end{cases}$$

To simplify the calculation, it is better to use the Euler angle method[34] in order to transform the coordinates from the (x', y', z') system to the (x, y, z) system (Figure 3). As a result the z-axis lies parallel to $\underset{\sim}{n}_0$ the normal of the disk.

In unprimed system (x, y, z) or (R, θ, Z),

$\gamma = R\cos\theta \, \hat{x} + R\sin\theta \, \hat{y} + Z \, \hat{z}$,

and

$$\underset{\sim}{k}\cdot\underset{\sim}{\gamma} = k_x R\cos\theta + k_y R\sin\theta + K_z Z$$

$$= |\underset{\sim}{k}|\sin\alpha\cos\beta_1\, R\cos\theta + |\underset{\sim}{k}|\sin\alpha\sin\beta_1\, R\sin\theta + |\underset{\sim}{k}|\cos\alpha\cdot Z$$

$$= |\underset{\sim}{k}|R\sin\alpha\,\cos(\theta-\beta_1) + |\underset{\sim}{k}|\cos\alpha\, z$$

and

$$\theta(\underset{\sim}{k}) = \int_0^{R_0}\int_0^{2\pi}\int_{-\frac{Z_0}{2}}^{\frac{Z_0}{2}} e^{i\underset{\sim}{k}\cdot\underset{\sim}{\gamma}}\, dR\, Rd\theta\, dz$$

$$= 2\int_0^{R_0}\int_{\beta_1}^{\pi+\beta_1}\int_{-\frac{Z_0}{2}}^{\frac{Z_0}{2}} \exp[i|\underset{\sim}{k}|R\sin\alpha\cos(\theta-\beta_1)+i|k|z\cdot\cos\alpha]RdRd\theta dz$$

(by symmetry argument)

setting $\theta' = \theta-\beta_1$, we have

$$\theta(\underset{\sim}{k}) = 2\int_0^{R_0}\int_0^{\pi} \frac{e^{i|\underset{\sim}{k}|R\sin\alpha\cos\theta'}\cdot 2\cdot\sin(|\underset{\sim}{k}|\cos\alpha\cdot\frac{Z_0}{2})}{|k|\cos\alpha}\, RdRd\theta'$$

$$= 4\,\frac{\sin(|\underset{\sim}{k}|\cos\alpha\cdot\frac{Z_0}{2})}{|\underset{\sim}{k}|\cos\alpha}\int_0^{R_0} \pi I_0(i|\underset{\sim}{k}|R\sin\alpha)\, RdR$$

$$= 2\pi Z_0\,\frac{\sin(|\underset{\sim}{k}|\cos\alpha\,\frac{Z_0}{2})}{(|\underset{\sim}{k}|\cos\alpha\cdot\frac{Z_0}{2})}\int_0^{R_0} J_0(|k|R\sin\alpha)\, RdR$$

$$= 2\cdot\underbrace{(\pi R_0^2 Z_0)}_{\substack{\text{volume}\\ \text{of the}\\ \text{inclusion}}}\,\frac{\sin(|\underset{\sim}{k}|\cos\alpha\cdot\frac{Z_0}{2})}{(|\underset{\sim}{k}|\cos\alpha\frac{Z_0}{2})}\cdot\frac{J_1(|\underset{\sim}{k}|\sin\alpha\cdot R_0)}{(|\underset{\sim}{k}|\sin\alpha R_0)}\,.$$

In the above derivations, we have used the following properties of Bessel functions:

$$\int_0^{\pi} e^{p\cos x} dx = \pi I_0(p)$$

$$I_0(ix) = J_0(-x) = J_0(x),$$

and

$$\int x^n J_{n-1} dx = x^n J_n .$$

It is clear that $\theta(\underset{\sim}{k})$ is independent of the coordinates chosen.

8. In k-space,

$$\underset{\sim}{n}_0 = (\sin\theta_0\cos\phi_0, \sin\theta_0\sin\phi_0, \cos\theta_0)$$

and

$$\underset{\sim}{n} = (\sin\theta\cos\phi, \sin\theta\sin\phi, \cos\theta).$$

Therefore, we have

$$\cos\alpha = \underset{\sim}{n}_0 \cdot \underset{\sim}{n} = \cos\theta\cos\theta_0 + \sin\theta\sin\theta_0 \cos(\phi_0 - \phi) .$$

9. In order to solve Eqs. (4-13) and (4-14), $f(n) = 0$ (see Eq. (4-8)) must be solved. To simplify the problem, several systems will be discussed.

(1) Al [40] $c_{11} = 1.082 \times 10^{12}$ ergs/cm^3

$c_{12} = 0.613 \times 10^{12}$ ergs/cm^3

$c_{44} = 0.285 \times 10^{12}$ ergs/cm^3 $\quad \Delta = -0.354$

If we set $y = n^2$, it follows directly from the range for n^2 that $0 \leqslant y \leqslant 1$. For $f(y)$, we get the expression

$$f(y) = f(n) = -y^3 + y^2 + 18.384y - 37.095,$$

from which it is easy to show that

$f(y) < 0$ for $0 \leq y \leq 1$.

(2) Cu [41] $c_{11} = 1.684 \times 10^{12}$ ergs/cm^3

$c_{12} = 1.214 \times 10^{12}$ ergs/cm^3

$c_{44} = 0.754 \times 10^{12}$ ergs/cm^3 $\Delta = -1.377$

$f(y) = -y^3 + y^2 + 0.13y - 0.239$

$f(y) < 0$ for $0 \leq y \leq 1$.

(3) Ni [41] $c_{11} = 2.465 \times 10^{12}$ ergs/cm^3

$c_{12} = 1.473 \times 10^{12}$ ergs/cm^3

$c_{44} = 1.247 \times 10^{12}$ ergs/cm^3 $\Delta = -1.204$

$f(y) = -y^3 + y^2 + 0.408y - 0.456$

$f(y) < 0$ for $0 \leq y \leq 1$.

(4) Nb[42] $c_{11} = 2.46 \times 10^{12}$ ergs/cm^3

$c_{12} = 1.34 \times 10^{12}$ ergs/cm^3

$c_{44} = 0.287 \times 10^{12}$ ergs/cm^3 $\Delta = 1.902$

$f(y) = -y^3 + y^2 + 1.881y + 0.567$

$f(y) > 0$ for $0 \leq y \leq 1$.

(5) Cr[43] $c_{11} = 3.5 \times 10^{12}$ ergs/cm^3

$c_{12} = 0.678 \times 10^{12}$ ergs/cm^3

$c_{44} = 1.008 \times 10^{12}$ ergs/cm^3 $\Delta = 0.8$

$f(y) = -y^3 + y^2 + 7.186y + 5.468$

$f(y) > 0$ for $0 \leq y \leq 1$.

Based on the results derived for the five cases above, it is very clear that in these cases, there are no other possible solutions for the mathematical extrema other than {111}, {001} and {011}.

10. For the Fe-C system, the elastic moduli are

$$c_{11} = 2.335 \times 10^{12} \text{ ergs/cm}^3 ,$$

$$c_{12} = 1.355 \times 10^{12} \text{ ergs/cm}^3 ,$$

and $c_{44} = 1.180 \times 10^{12}$ ergs/cm^3 .

The following parameters can be obtained from Eqs. (2-42), (2-51a), (2-51b) and (2-52a) by substituting the values of the elastic constants:

$$\Delta = -1.169$$

$$\sigma_0 = 1.137 \times 10^{12} (x_c) \text{ ergs/cm}^3 ,$$

$$\tilde{\sigma}_0 = 0.62 \times 10^{12} (x_c) \text{ ergs/cm}^3 ,$$

$$A = -0.05 ,$$

$$B = -0.828 ,$$

$$C = -0.486 ,$$

and $\gamma = 0.471$.

11. The orientation of the disk normal (0.383, 0, 0.924) with respect to the minimum elastic strain energy in the Fe-N system was obtained with the same method as that used for the Fe-C system.

12. The Fourier transform of $u_{ij}(\underset{\sim}{r})$ $(= \frac{\partial u_i(\underset{\sim}{r})}{\partial \gamma_j})$ is

$$\begin{aligned} u_{ij}(\underset{\sim}{k}) &= ik_j u_i(\underset{\sim}{k}) \\ &= ik_j(-i)(\underset{\approx}{G}\,\underset{\approx}{\sigma}^0)_{il}\, k_l\, \theta(\underset{\sim}{k}) \\ &= n_j\, (\underset{\approx}{\Omega}\,\underset{\approx}{\sigma}^0)_{il}\, n_l\, \theta(\underset{\sim}{k}) . \end{aligned}$$

Transforming $u_{ij}(k)$ back to real space, $u_{ij}(\gamma)$ can be expressed as

$$u_{ij}(\underset{\sim}{\gamma}) = \int \frac{d^3k}{(2\pi)^3} e^{i\underset{\sim}{k}\cdot\underset{\sim}{\gamma}} n_j (\underset{\approx}{\Omega}\,\underset{\approx}{\sigma}^0)_{il} n_l \theta(\underset{\sim}{k}) .$$

For a thin plate with a normal equal to $\underset{\sim}{n}_0$, the following approximation can be made.

$$u_{ij}(\underset{\sim}{\gamma}) \approx n_j^0 (\underset{\approx}{\Omega}\,\underset{\approx}{\sigma}^0)_{il} n_l^0 \int \frac{d^3k}{(2\pi)^3} e^{i\underset{\sim}{k}\cdot\underset{\sim}{\gamma}} \theta(\underset{\sim}{k})$$

$$= n_j^0 (\underset{\approx}{\Omega}\,\underset{\approx}{\sigma}^0)_{il} n_l^0 \theta(\underset{\sim}{\gamma}) .$$

For the Fe-N system, (001) has been proved to be the orientation of the disk-shaped inclusion normal with respect to the minimum elastic strain energy. From Eqs. (2-41) and (2-42), we have

$$\underset{\approx}{\Omega}(001) = \begin{pmatrix} \frac{1}{C44} & 0 & 0 \\ 0 & \frac{1}{C44} & 0 \\ 0 & 0 & \frac{1}{C11} \end{pmatrix} .$$

From Eq. (5-2), we get

$$\sigma_{ij}^0 = \lambda_{ij\ell m} \varepsilon_{\ell m}^0 = X_N \begin{pmatrix} -0.095C11+0.76C12 & 0 & 0 \\ 0 & -0.095C11+0.76C12 & 0 \\ 0 & 0 & 0.855C11-0.19C12 \end{pmatrix} .$$

Therefore, inside the inclusion

$$u_{ij} = n_j^0 (\underset{\approx}{\Omega}\,\underset{\approx}{\sigma}^0)_{il}\, n_\ell^0$$

$$= \begin{pmatrix} 0 & 0 & 0 \\ 0 & 0 & 0 \\ 0 & 0 & 0.855-0.19\frac{C12}{C11} \end{pmatrix} X_N$$

$$u_{33} = \varepsilon_{33} = (0.855 - 0.19\,\frac{1.355}{2.355})\,\frac{1}{8} = 0.093$$

$$u_{11} = u_{22} = \varepsilon_{11} = \varepsilon_{22} = 0$$

From this it follows that the crystal lattice parameters of the tetragonal α'' ($Fe_{16}N_2$) phase, which is itself a superlattice in the BCC lattice of αFe phase, are (see Figure 6)

$$c = 2a_0 + \Delta c = 2a_0 + 2a\cdot\varepsilon_{33} = 6.263\ \text{Å}$$

$$a = 2a_0 + \Delta a = 2a_0 + 2a_0\cdot\varepsilon_{11} = 5.73\ \text{Å}$$

These results are in good agreement with experimentally determined crystal lattice parameters of the α'' phase,[38]

$$c_{\alpha''} = 6.29\ \text{Å}$$

$$a_{\alpha''} = b_{\alpha''} = 5.73\ \text{Å}$$

TABLE I: Fe-N System. $\phi_0 = 0$.

	Z_0	R_0	$z_0/2R_0$	θ_0	Orientation
1.	10	50	1/10	0	[001]
2.	9.5	51.299	1/10.8	0	[001]
3.	9.25	51.9875	1/11.24	0	[001]
4.	9.2	52.1286	1/11.34	0	[001]
5.	9.1	52.4142	1/11.52	1.65°	[0.029, 0, 0.996]
6.	9.0	52.704	1/11.71	2.95°	[0.051, 0, 0.999]
7.	7.5	57.735	1/15.38	10.35°	[0.180, 0, 0.984]
8.	5.0	70.71	1/28.28	15.94°	[0.275, 0, 0.962]
9.	2.5	100.	1/80	19.47°	[0.333, 0, 0.943]
10.	0	-	0	22.5	[0.382, 0, 0.924]

*Cases with $\phi_0 \neq 0$ were calculated, and they showed the similar results.

REFERENCES

1. A.G. Khachaturyan and R.A. Suris, Sov. Phys. Crystallography 13. 63 (1968).
2. A.G. Khachaturyan and G.A. Shatalov, Sov. Phys. Solid State 11, 118 (1969).
3. A.G. Khachaturyan, Sov. Phys. JETP 31, 98 (1970).
4. A.G. Khachaturyan, Phys. Stat. Sol. 35, 119 (1969).
5. A.G. Khachaturyan and V.M. Airapetyan, Phys. Stat. Sol. (A) 26, 61 (1974).
6. J.D. Eshelby, Appendix to article by A.J. Ardell and R.B. Nicholson, Acta Met. 14, 1295 (1966).
7. L.M. Brown, et al, Scripta Met. 7,815 (1973).
8. P.H. Eurin, J.M. Penisson and A. Bourret, Acta Met. 21, 559 (1975).
9. S. Nagakura, K. Shiraishi and Y. Hirotsu, Trans. JIM 16, 601 (1975).
10. J.D. Eshelby, Proc. Roy. Soc. A241, 376 (1957).
11. J.D. Eshelby, Proc. Roy. Soc. A252, (1959).
12. J.D. Eshelby, Progress in Solid Mechanics 2, 89 (1961).
13. L.J. Walpole, Proc. Roy. Soc. A300, 270 (1967).
14. N. Kinoshita and T. Mura, Phys. Status Sol. 25, 759 (1971).
15. R.J. Asaro and D.M. Barnett, J. Mech. Phys. Solids 23, 77 (1975).
16. J.K. Lee, D.M. Barnett and H.I. Aaronson, Met. Trnas., 8A, 963 (1977).
17. A.G. Khachaturyan, Sov. Phy. Solid State 8, 2163 (1967).
18. A.G. Khachaturyan, Sov. Phys. Solid State 9, 2249 (1968).
19. M.A. Krivoglaz, The Theory of X-Ray and Thermal Neutron Diffraction Scattering by Real Crystals, Chapter 2, Plenum Press, 1969.
20. M. Born and K. Huang, Dynamical Theory of Crystal Lattices, (Oxford University Press, 1954).
21. J.M. Zinman, Principles of the Theory of Solids, Chapter 2, second edition, Cambridge University Press, 1972.

22. N.W. Ashcroft and N.D. Mermin, Solid State Physics, Chapter 22, Holt, Rinehart and Winston, 1976.

23. P. Schewillinger, H.J. Leamy and Warlimont, Acta Met. 19, 421 (1971).

24. R.D. Garwood and G. Thomas, Met. Trans. 4, 225 (1973).

25. Nye, Physical Properties of Crystals, Chapter 8, Oxford, Clarendon Press, 1957.

26. R.B. Nicholson and J. Nutting, Acta Met. 9, 332 (1961).

27. V.A. Phillips and J.D. Livingston, Phil. Mag. 7, 969 (1962).

28. V.A. Phillips, Acta Met. 21, 219 (1973).

29. V.A. Phillips and L. Tanner, Acta Met. 21, 441 (1973).

30. R. Cozar and A. Pineau, Met. Trans. 4, 47 (1973).

31. J.M. Oblak, D.F. Paulonis and D.S. Duvall, Met. Trans. 5, 143 (1974).

32. C. Ravindran and M.C. Chaturvedi, Met. Trans. 6A, 213 (1975).

33. H.F. Merrick, Met. Trans. 7A, 505 (1976).

34. H. Goldstein, Classical Mechanics, Chapter 4, Addison-Wesley, 1950.

35. C.S. Roberts, Trans. AIME, 197, 203 (1953).

36. V.I. Izotov and L.M. Uterskiy, Phys. Met. and Metallog. 25, 98 (1968).

37. T. Bell and W.S. Owen, JISI, 205, 428 (1967).

38. K.H. Jack, Proc. Roy. Soc. A208, 200 (1951).

39. K.H. Jack, ibid., 216.

40. P.M. Sutton, Phys. Rev. 91, 816 (1953).

41. H.B. Huntington, Solid State Phys. 7, 213 (1958).

42. D. Bolef, J. Appl. Phys. 32, 100 (1961).

43. D. Bolef and J. deKlerk, Phys. Rev. 129, 1063 (1965).

44. S. Oketani, S. Hitomi and S. Nagakura, J. Japan Inst. Metals, 26, 994 (1962) (in Japanese).

45. P.G. Winchell and M. Cohen, Trans. Am. Soc. Metals 55, 347 (1962).

46. J.M.R. Genin and P.A. Flinn, Trans. Met. Soc. AIME, 242, 1419 (1968).

47. A.G. Khachaturyan and T.A. Onisimova, Phys. Met. and Metallog. 26, 12 (1968).

FIGURE CAPTIONS

Fig. 1: Disk-shaped inclusion with radius R_0, thickness Z_0, and normal $\underset{\sim}{n}_0$.

Fig. 2: Disk-shaped inclusion sitting in the primed system (x', y', z').

Fig. 3: The coordinates are transformed by the Euler angle method from the (x', y', z') system to the (x, y, z) system in which $\underset{\sim}{n}_0$ is parallel to $\underset{\sim}{Z}$.

Fig. 4: Plotting of $\frac{(\underset{\sim}{k})}{V}$ vs. α for

(1) $|\underset{\sim}{k}| = 1$, $Z_0 = 2.5$, $R_0 = 100$,

(2) $|\underset{\sim}{k}| = 1$, $Z_0 = 5$, $R_0 = 70.71$,

(3) $|\underset{\sim}{k}| = 1$, $Z_0 = 10$, $R_0 = 50$.

Fig. 5: Plotting of $B(\theta,\phi)$ vs. θ for Al-Cu system shows the minimum at $\theta = 0^0$.

Fig. 6: Ordered structure of $Fe_{16}N_2$.

Fig. 7: Plotting of function $\omega(n_3)$ defined in Eq. (5-14).

Fig. 8: Plotting of $B(\theta,\phi)$ vs. θ for Fe-N system.

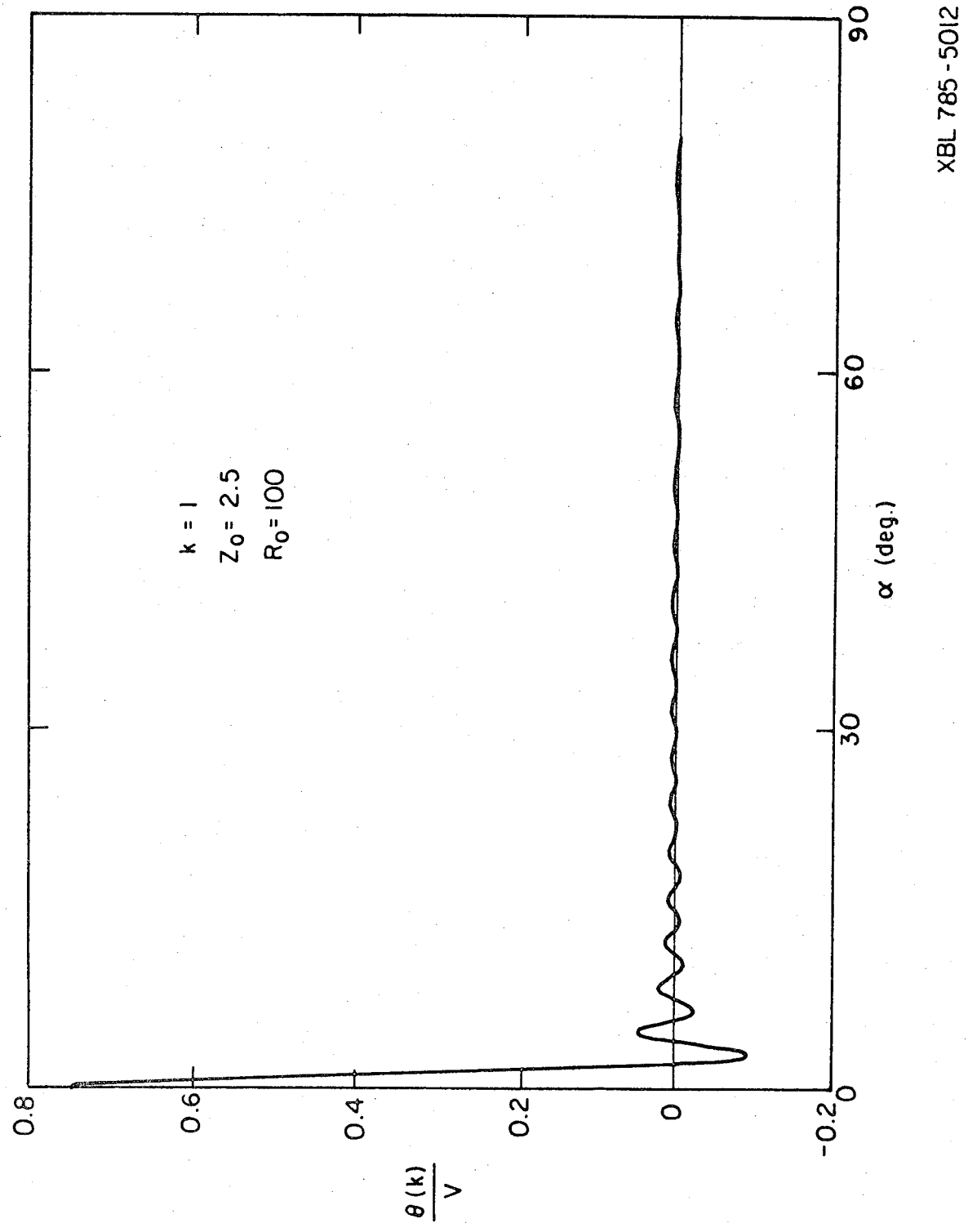
k = 1
Z_o= 2.5
R_o=100
0.8
0.6
0.4
0.2
0
-0.2
0
30
60
90
α (deg.)
$\frac{\theta(k)}{V}$
XBL 785-5012

Figure 4-1

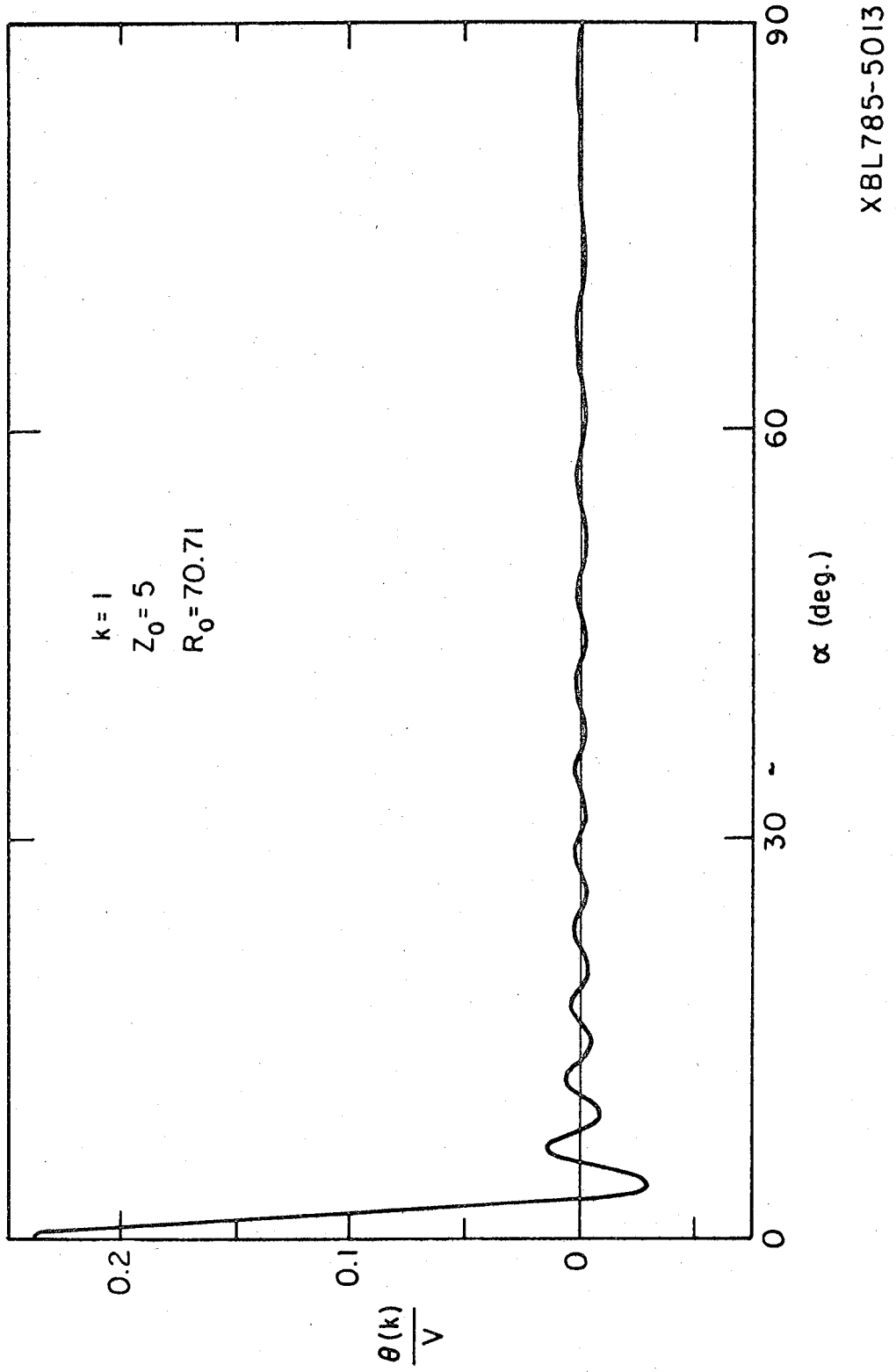

Figure 4-2

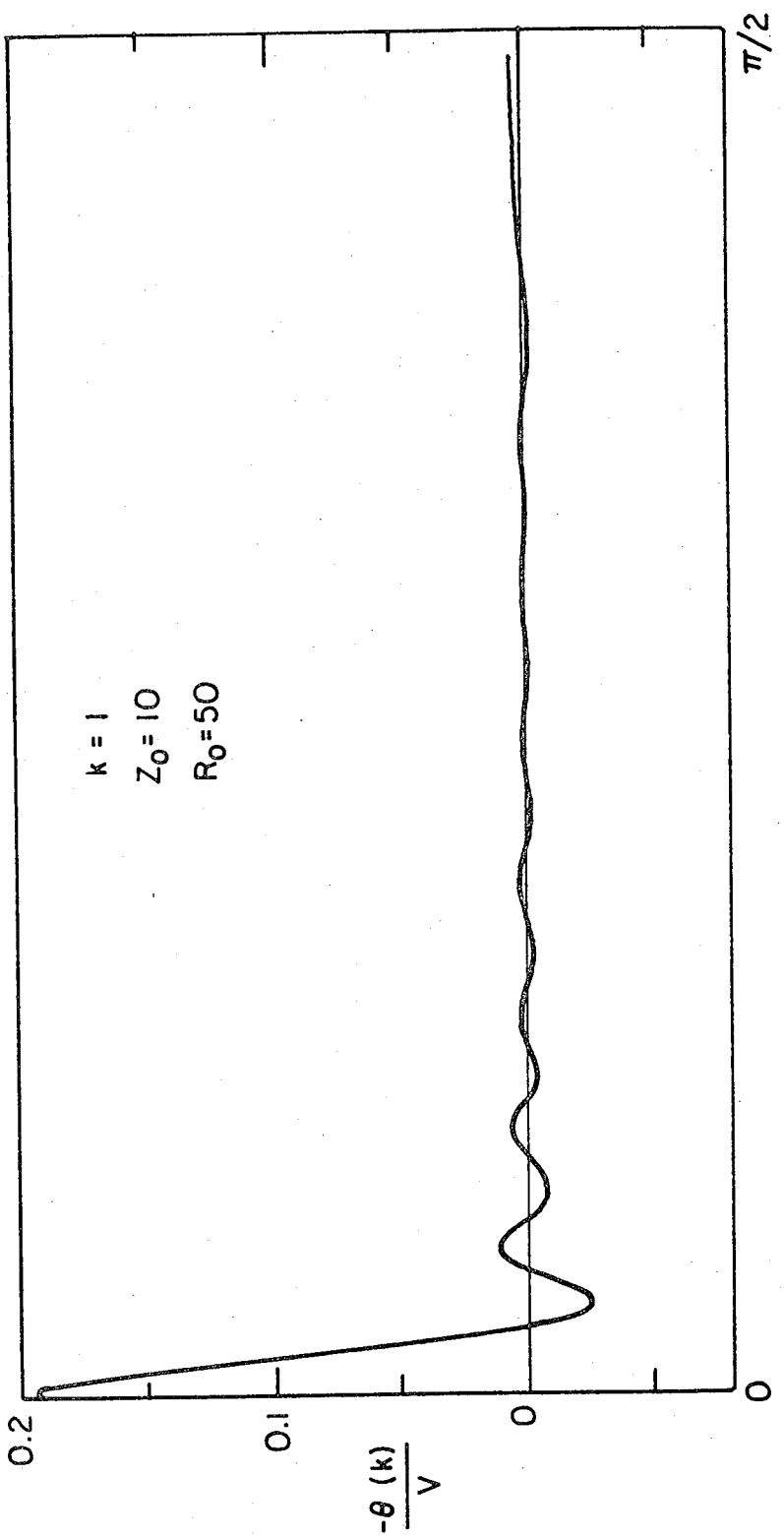

Figure 4-3

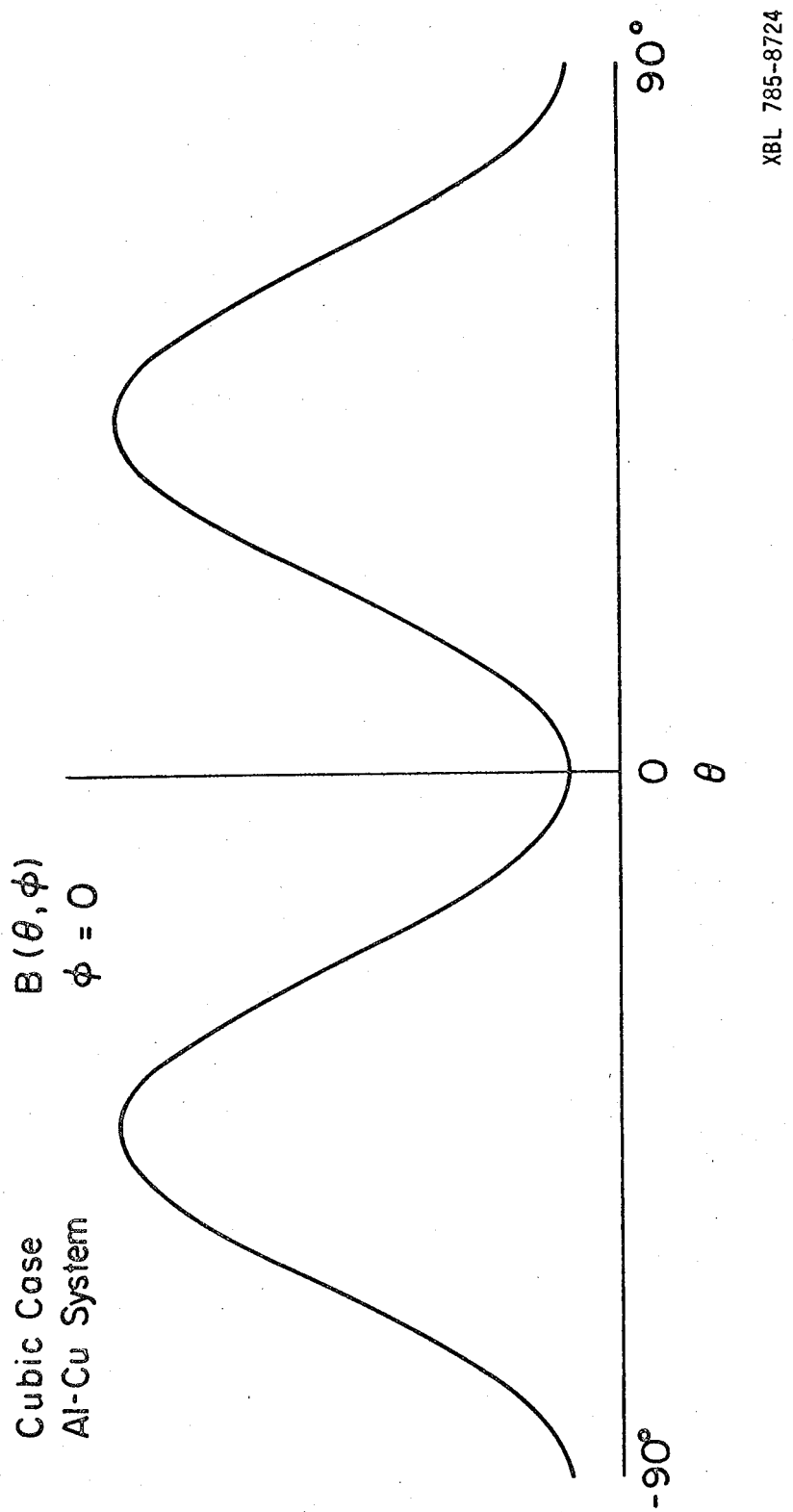

Figure 5

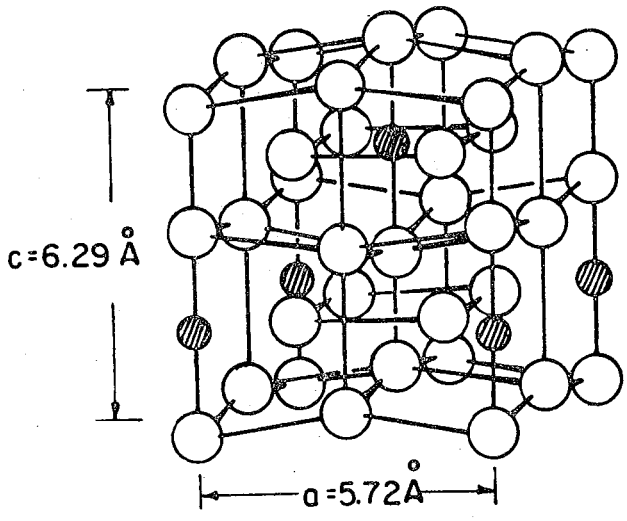

XBL 785-5014

Figure 6

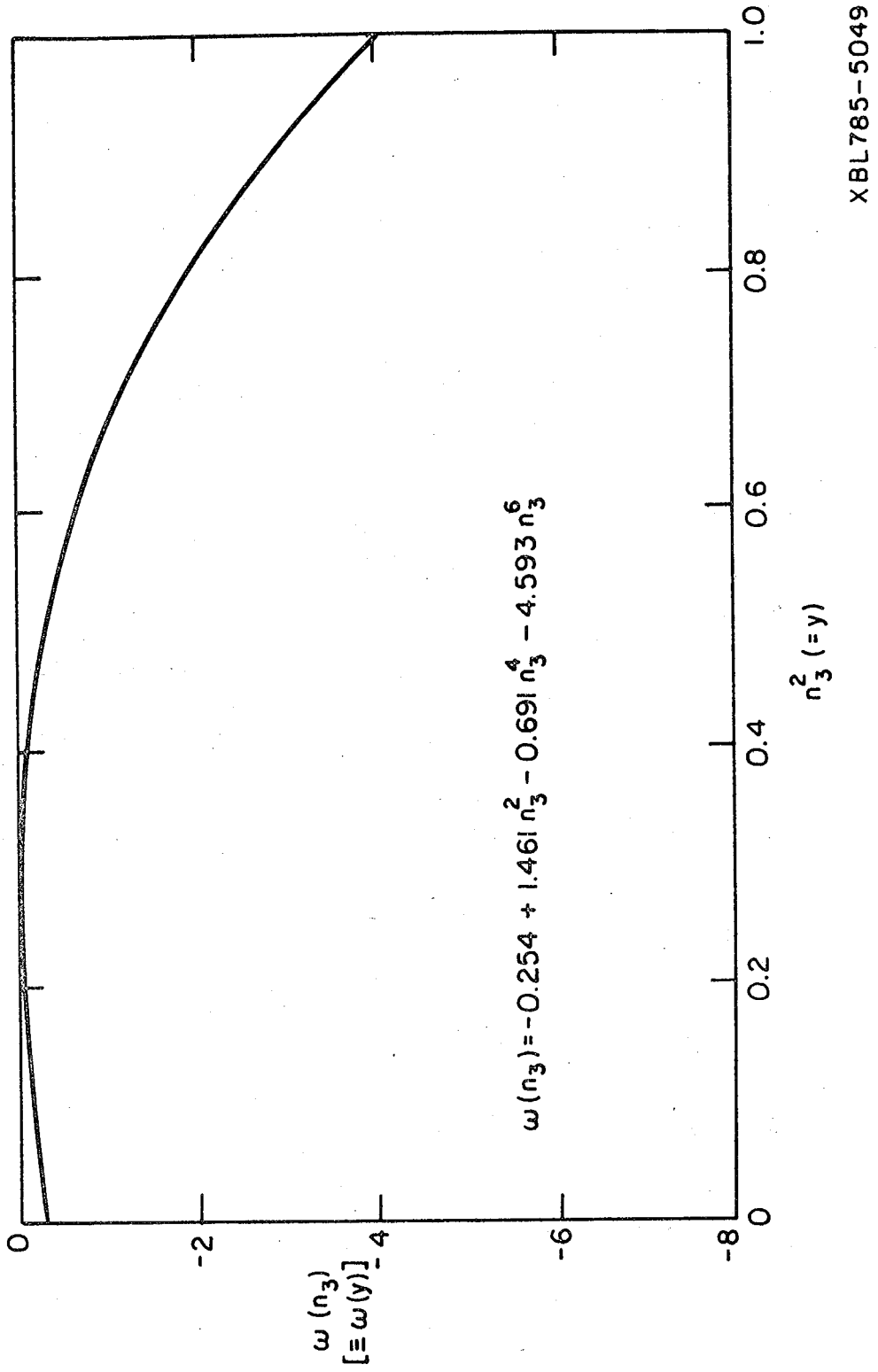

Figure 7

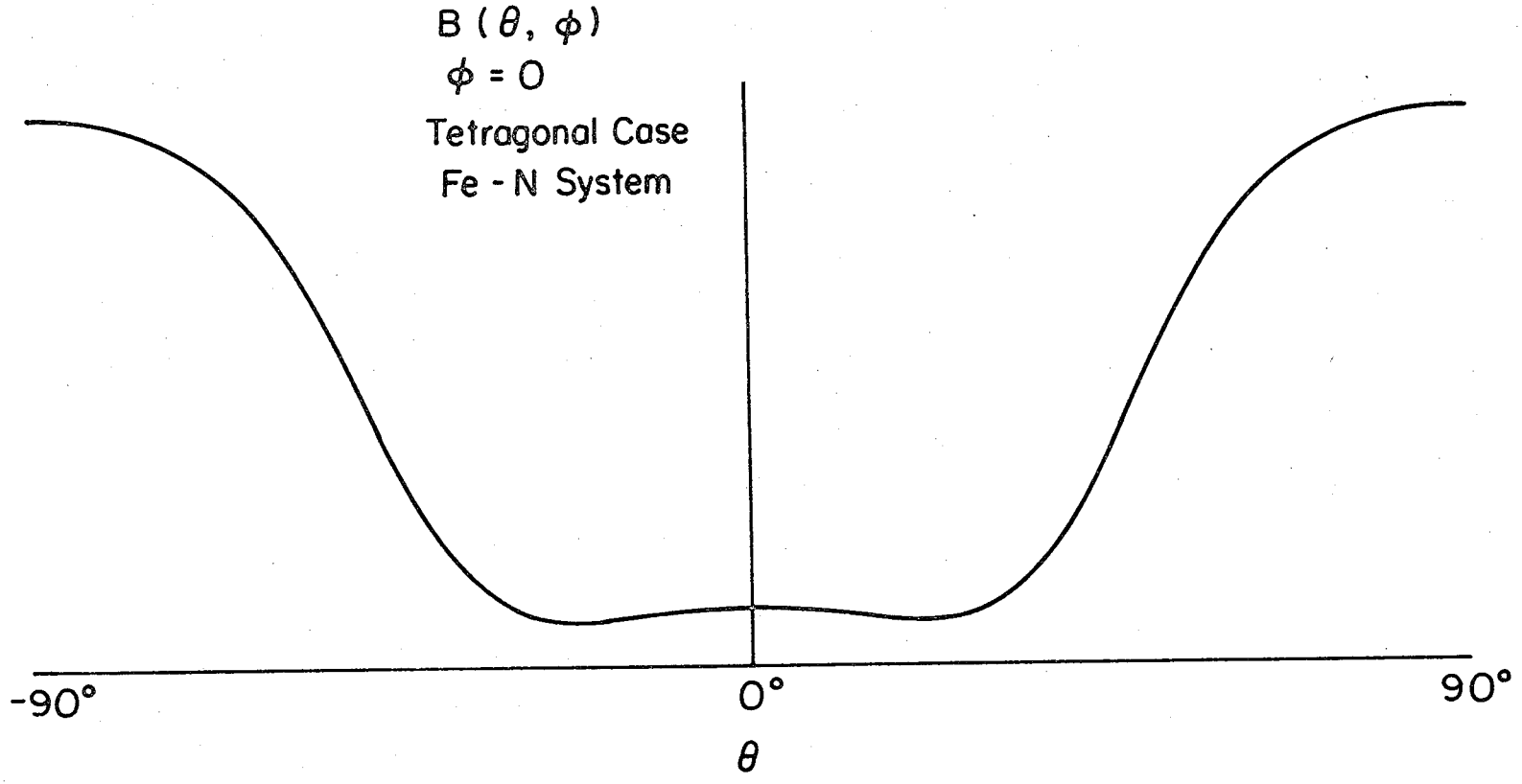

XBL 785-8723

Figure 8

This report was done with support from the Department of Energy. Any conclusions or opinions expressed in this report represent solely those of the author(s) and not necessarily those of The Regents of the University of California, the Lawrence Berkeley Laboratory or the Department of Energy.